AMERICAN SOCIETY FOR MICROBIOLOGY | Applied and Environmental Microbiology®

PHYSIOLOGY

Role of *N,N*-Dimethylglycine and Its Catabolism to Sarcosine in *Chromohalobacter salexigens* DSM 3043

Ting Yang,[a] Ya-Hui Shao,[b] Li-Zhong Guo,[a] Xiang-Lin Meng,[a] Hao Yu,[a] Wei-Dong Lu[a]

[a]Shandong Provincial Key Laboratory of Applied Mycology, College of Life Sciences, Qingdao Agricultural University, Qingdao, People's Republic of China
[b]Biotechnology Research Institute, Chinese Academy of Agricultural Sciences, Beijing, People's Republic of China

Ting Yang, Ya-Hui Shao, and Li-Zhong Guo contributed equally to this work. Author order was determined according to the innovation of their experimental results.

ABSTRACT *Chromohalobacter salexigens* DSM 3043 can grow on *N,N*-dimethylglycine (DMG) as the sole C, N, and energy source and utilize sarcosine as the sole N source under aerobic conditions. However, little is known about the genes and enzymes involved in the conversion of DMG to sarcosine in this strain. In the present study, gene disruption and complementation assays indicated that the *csal_0990*, *csal_0991*, *csal_0992*, and *csal_0993* genes are responsible for DMG degradation to sarcosine. The *csal_0990* gene heterologously expressed in *Escherichia coli* was proven to encode an unusual DMG dehydrogenase (DMGDH). The enzyme, existing as a monomer of 79 kDa with a noncovalently bound flavin adenine dinucleotide, utilized both DMG and sarcosine as substrates and exhibited dual coenzyme specificity, preferring NAD^+ to $NADP^+$. The optimum pH and temperature of enzyme activity were determined to be 7.0 and 60°C, respectively. Kinetic parameters of the enzyme toward its substrates were determined accordingly. Under high-salinity conditions, the presence of DMG inhibited growth of the wild type and induced the production and accumulation of trehalose and glucosylglycerate intracellularly. Moreover, exogenous addition of DMG significantly improved the growth rates of the four DMG^- mutants (Δ*csal_0990*, Δ*csal_0991*, Δ*csal_0992*, and Δ*csal_0993*) incubated at 37°C in S-M63 synthetic medium with sarcosine as the sole N source. ^{13}C nuclear magnetic resonance (^{13}C-NMR) experiments revealed that not only ectoine, glutamate, and *N*-acetyl-2,4-diaminobutyrate but also glycine betaine (GB), DMG, sarcosine, trehalose, and glucosylglycerate are accumulated intracellularly in the four mutants.

IMPORTANCE Although *N,N*-dimethylglycine (DMG) dehydrogenase (DMGDH) activity was detected in cell extracts of microorganisms, the genes encoding microbial DMGDHs have not been determined until now. In addition, to our knowledge, the physiological role of DMG in moderate halophiles has never been investigated. In this study, we identified the genes involved in DMG degradation to sarcosine, characterized an unusual DMGDH, and investigated the role of DMG in *Chromohalobacter salexigens* DSM 3043 and its mutants. Our results suggested that the conversion of DMG to sarcosine is accompanied by intramolecular delivery of electrons in DMGDH and intermolecular electron transfer between DMGDH and other electron acceptors. Moreover, an unidentified methyltransferase catalyzing the production of glycine betaine (GB) from DMG but sharing no homology with the reported sarcosine DMG methyltransferases was predicted to be present in the cells. The results of this study expand our understanding of the physiological role of DMG and its catabolism to sarcosine in *C. salexigens*.

KEYWORDS *Chromohalobacter salexigens*, metabolism, *N,N*-dimethylglycine, dimethylglycine dehydrogenase, flavoprotein, compatible solute

Citation Yang T, Shao Y-H, Guo L-Z, Meng X-L, Yu H, Lu W-D. 2020. Role of *N,N*-dimethylglycine and its catabolism to sarcosine in *Chromohalobacter salexigens* DSM 3043. Appl Environ Microbiol 86:e01186-20. https://doi.org/10.1128/AEM.01186-20.

Editor Haruyuki Atomi, Kyoto University

Address correspondence to Wei-Dong Lu, luweidong401@hotmail.com.

Received 19 May 2020
Accepted 28 June 2020
Accepted manuscript posted online 6 July 2020
Published 18 August 2020

Glycine betaine (*N*,*N*,*N*-trimethylglycine; GB), a compound that is ubiquitous in nature, not only functions as an effective compatible solute to cope with osmotic and other abiotic stresses in members of all three domains of life but also serves as a nutrient for a considerable number of microorganisms or as the methyl group donor in some mammalian cells. In some symbiotic and pathogenic bacteria, such as *Sinorhizobium meliloti* and *Pseudomonas aeruginosa*, catabolism of GB improves the competitiveness of strains in the rhizosphere or contributes to their infectious potential when forming close associations with their eukaryotic hosts (1–3). Recent studies have indicated that GB also plays an important role as a regulator in cellular metabolism, such as ethanol, carbohydrate, lipid, and homocysteine/methionine metabolism (4).

As a nutrient utilized by many *Bacteria* and even some *Archaea*, GB can be catabolized either aerobically or anaerobically. Under anaerobic conditions, GB is either reduced by GB reductase to yield trimethylamine (TMA) and acetate, as represented by some species of the genus *Clostridium* (5, 6), or demethylated by GB methyltransferase to produce *N*,*N*-dimethylglycine (DMG), which is further metabolized to acetate and butyrate, as typically found in *Eubacterium limosum* (7) and methanogenic *Methanococcoides* strains (8). Recently, Lechtenfeld et al. reported that in *Acetobacterium woodii*, GB is catabolized through the Wood-Ljungdahl pathway with DMG and acetate as the end products (9). Under aerobic conditions, catabolism of GB proceeds with sequential removal of its methyl groups, producing DMG, sarcosine, and glycine in consecutive steps. However, the enzymes that catalyze each reaction come from different enzyme families in different species of microorganisms. In the first step of the GB degradation pathway, GB is converted to DMG by either betaine-homocysteine methyltransferases (BHMT, EC 2.1.1.5) or GB monooxygenases, as represented by *S. meliloti* 102F34 (1) or *Chromohalobacter salexigens* DSM 3043 (10), respectively. In the second step, DMG is oxidized to sarcosine by DMG oxidases (DMGO, EC 1.5.3.10), as reported in *Cylindrocarpon didymum* M-1 (11) and *Arthrobacter globiformis* (12), which share amino acid sequence similarities with those of mammalian DMG dehydrogenases (EC 1.5.8.4, formerly EC 1.5.99.2). In the third step, sarcosine is further oxidized to glycine either by sarcosine dehydrogenase (SDH), as reported in *Pseudomonas putida* (13) and *Pseudomonas fluorescens* (14), or by one of two different types of sarcosine oxidases (SOX, EC 1.5.3.1), monomeric sarcosine oxidase (MSOX) or heterotetrameric sarcosine oxidase (TSOX), as typically found in *Bacillus* sp. strain B-0618 (15) and *Pseudomonas maltophilia* (16), respectively. In some mammals, GB is metabolized to glycine in the mitochondria of liver cells via three *N*-demethylation reactions catalyzed by BHMT, mammalian DMGDH, and SDH, respectively (17).

Besides GB and ectoine, precursors of these osmolytes can provide osmotic and/or thermal stress protection for some bacteria under external stress conditions, as shown in recent studies. *N*-Acetyl-2,4-diaminobutyrate (NADA), the precursor of ectoine, is accumulated intracellularly and functions as an osmoprotectant for the nonhalophilic bacterium *Salmonella enterica* serovar Typhimurium, although its osmoprotective effect is slightly lower than that of ectoine (18). DMG, which is a metabolic intermediate in the GB biosynthetic and catabolic pathway, as well as in the choline and carnitine degradation pathway (19), is accumulated in *Yersinia enterocolitica* ATCC 9610 under osmotic stress conditions, and its ability to alleviate the effects of salinity on the growth of *Y. enterocolitica* is about 90% that of GB (20). In *Bacillus subtilis*, the ability to take up DMG from exogenous sources confers osmotic and thermal tolerance to cells exposed to stressful environmental conditions (21).

C. salexigens DSM 3043 is considered an excellent model organism for studying the molecular basis of prokaryotic osmoregulation due to the ability of this bacterium to grow in a wide range of salt concentrations, from 0.15 M to 4.3 M NaCl, and its simple nutrient requirements for growth (22, 23). Unlike *E. coli* and *B. subtilis*, *C. salexigens* DSM 3043 can utilize GB not only as an effective osmolyte but also as a nutrient through three *N*-demethylation reactions (Fig. 1). Recently, a Rieske-type GB monooxygenase was identified to catalyze the first step of the GB degradation pathway in *C. salexigens* (10). Gene deletion experiments indicated that the four open reading frames (ORFs)

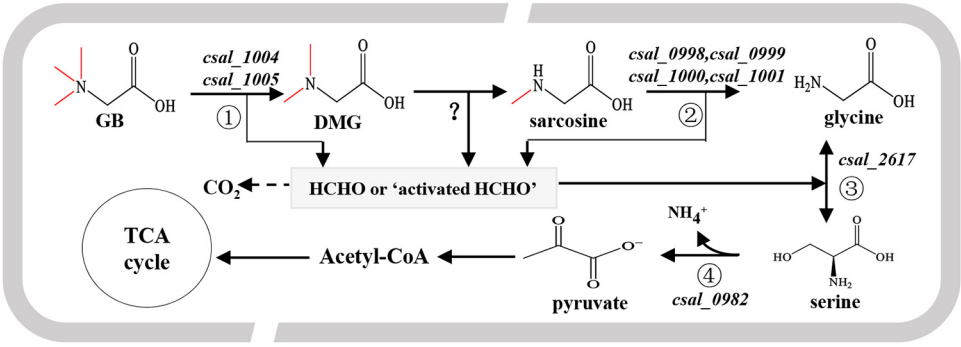

FIG 1 GB degradation pathway in *C. salexigens* DSM 3043. (1) Glycine betaine monooxygenase encoded by the *csal_1004* and *csal_1005* genes catalyzes the conversion of GB to DMG. (2) Heterotetrameric sarcosine oxidase encoded by the *csal_0998*, *csal_0999*, *csal_1000*, and *csal_1001* genes catalyzes the oxidative *N*-demethylation of sarcosine to glycine. (3) Serine hydroxymethyltransferase encoded by the *csal_2617* gene catalyzes the reversible conversion of glycine to serine. (4) L-Serine ammonia lyase encoded by the *csal_0982* gene catalyzes the conversion of L-serine to pyruvate and ammonia. TCA cycle, the tricarboxylic acid cycle or the Krebs cycle. The question mark represents an uncharacterized enzyme catalyzing the conversion of DMG to sarcosine in *C. salexigens*.

csal_0998, *csal_0999*, *csal_1000*, and *csal_1001*, encoding the predicted β, δ, α, and γ subunits, respectively, of heterotetrameric sarcosine oxidase, are involved in GB catabolism (24). However, the enzyme responsible for catalyzing the conversion of DMG to sarcosine has not been identified, and its catalytic mechanism is still unknown. In addition, as an important intermediate in GB, choline, carnitine, and one-carbon-compound catabolism, the physiological role of DMG in halophilic bacteria has not yet been explored. In the present study, genetic and biochemical data indicated that the *csal_0990* gene encodes an unusual DMGDH and that exogenous addition of DMG induces production and accumulation of trehalose, glucosylglycerate (GG), and GB intracellularly in *C. salexigens*.

RESULTS

DMG inhibits growth of *C. salexigens* rather than functioning as an osmoprotectant. We previously showed that *C. salexigens* DSM 3043 is able to grow on DMG but not on sarcosine or glycine as the sole C source (10). In this study, we found that sarcosine and glycine, as well as DMG, could be used as the sole N source by strain ZW4-1, a spontaneous rifampin-resistant (Rif^r) mutant of *C. salexigens* DSM 3043, suggesting that the cells can transport sarcosine and glycine from the extracellular environment (see Fig. S1 in the supplemental material). To investigate whether DMG has any osmoprotective effect on the growth of ZW4-1, DMG (5 mM) was added to S-M63 medium containing 1 M NaCl. As shown in Fig. 2A, the higher the salinity in the medium, the stronger the inhibitory effect of DMG on the growth of ZW4-1. Interestingly, DMG showed a slight osmoprotective effect on cell growth during the first 8 h after inoculation. To further investigate whether the inhibition is due to intracellular accumulation of DMG, the cells grown in S-M63 containing 2 M NaCl and DMG were collected, and then their intracellular solutes were extracted. ^{13}C nuclear magnetic resonance (NMR) spectral analysis revealed that not only ectoine, glutamate, and NADA but also trehalose and GG were accumulated in the cells. However, the peaks belonging to DMG were absent, and the signals of hydroxyectoine were very faint under these conditions (Fig. 2B). In contrast, trehalose and GG were not detected in the intracellular compatible solute pools of the cells grown in M63 medium containing NaCl at concentrations ranging from 0.75 M to 2.5 M (25).

Identification and sequence analysis of the genes involved in DMG degradation to sarcosine in *C. salexigens*. To identify the gene(s) responsible for the conversion of DMG to sarcosine, a homology search was performed within the genome of *C. salexigens* DSM 3043 (GenBank accession number NC_007963.1) using two dimethylglycine oxidases (DMGO) from *Arthrobacter globiformis* (AAK16482.1 and ABB73054.1)

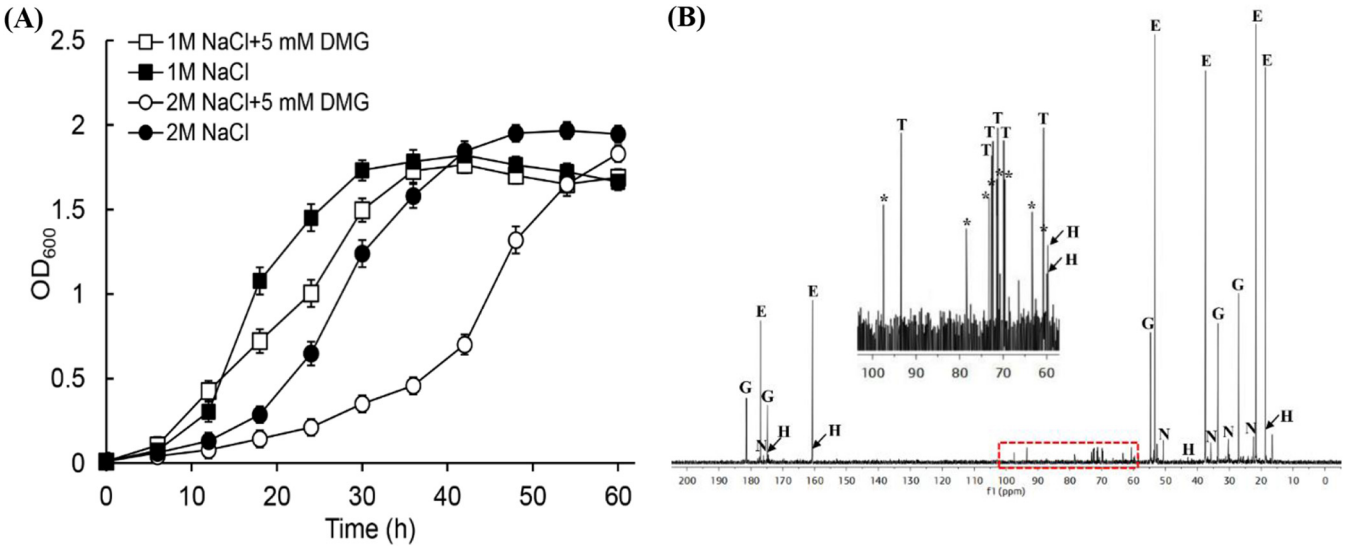

FIG 2 Effect of DMG on the growth of *C. salexigens* ZW4-1 and its intracellular accumulation of compatible solutes. (A) Growth of ZW4-1 at 37°C in S-M63 liquid medium containing different NaCl concentrations in the presence or absence of exogenous additive DMG. (B) ^{13}C-NMR spectra for the major cytosolic solutes of ZW4-1 cells grown at 37°C in S-M63 containing 2 M NaCl and DMG. The inset is a partially enlarged view of the area of the figure marked by red dotted lines. The signals are as follows: ectoine (E), hydroxyectoine (H), glutamate (G), NADH (N), trehalose (T), and glucosylglycerate (*).

(12), a human DMGDH (NP_037523.2) (17), and the predicted PA5398 (*dgcA*) and PA5399 (*dgcB*) products (NP_254085.1 and NP_254086.1) from *P. aeruginosa* PAO1 (26) as query sequences. No protein homologs of the bacterial DMGO and human DMGDH were found, but two adjacent ORFs, *csal_0990* and *csal_0991*, were returned as the top hit, which have 90% and 84% sequence similarity to the *dgcA* and *dgcB* products, respectively. The two genes in *P. aeruginosa* were previously shown to be responsible for DMG degradation to sarcosine, since transposon insertion in the two genes made the mutants defective in growth on DMG as the sole C source (26).

csal_0990 encodes a putative 694-amino-acid polypeptide. Signal and transmembrane peptides were not found in its putative gene product (DdhC), suggesting a cytoplasmic localization of the protein. Inspection of the primary structure of DdhC revealed the presence of a conserved dinucleotide-binding motif [GXGX$_2$(G/A)X$_{17}$(D/E), where X represents any amino acid residue] from residues 397 to 402, which is considered part of the Rossmann fold (27). As one of the three most highly represented folds in the Protein Data Bank (PDB), the Rossmann fold that binds FAD or NAD(P)H typically contains the conserved motif. Therefore, DdhC probably functions as an oxidoreductase.

csal_0991, which is located 181 bp downstream of *csal_0990*, encodes a putative 670-amino-acid protein. Sequence alignments indicated that the putative gene product (Csal0991) contains two [4Fe-4S] cluster-binding motifs (CX$_2$CX$_2$CX$_3$CP, where X represents any amino acid residue) (Fig. S2), which is a distinctive characteristic of the clostridial-type ferredoxins (28). In addition, analysis of Csal0991 with the programs TMpred and TMHMM revealed that five transmembrane regions are located at the N terminus of the enzyme (Fig. S3). Therefore, Csal0991 is likely to be a transmembrane "clostridial-type" ferredoxin.

The genes *csal_0992* and *csal_0993*, located directly downstream of *csal_0991*, encode two putative proteins with molecular masses of 44.7 and 28.5 kDa, respectively. There are 4 bp and 11 bp of overlapping nucleotides between *csal_0991* and *csal_0993*, respectively, suggesting that the three genes might be organized in an operon and translationally coupled. A BLASTP search demonstrated that the *csal_0992* gene product shares 77% sequence similarity with the α subunit of electron transfer flavoprotein (ETF) from *Agrobacterium tumefaciens* S33, while the *csal_0993* gene product shares 78% sequence similarity with the β subunit of ETF from *Agrobacterium tumefaciens* S33

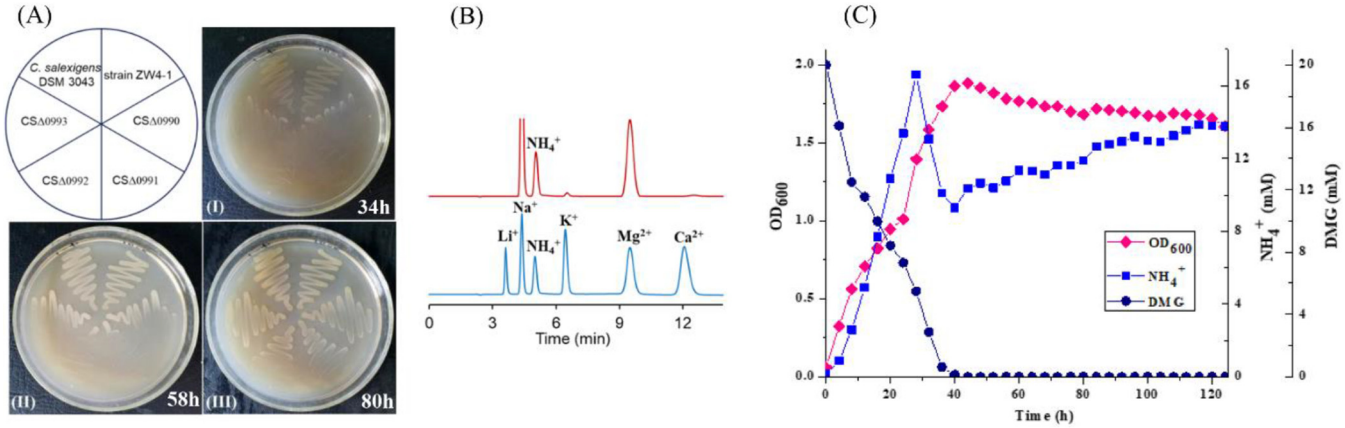

FIG 3 Catabolism of DMG by strain ZW4-1 resulted in release of ammonium. (A) Commensalism occurring between ZW4-1 and the four mutants. (B) Ion chromatography spectra for the supernatant of culture broth (red line) and cationic standards (blue line). (C) Time course of DMG and ammonium concentrations in the culture medium (S-M63 plus 1 M NaCl with DMG as the sole N source) inoculated with strain ZW4-1. Error bars represent the standard deviations (SD) of two independent experiments.

(29). Therefore, *csal_0992* and *csal_0993* were designated *etfA* and *etfB*, respectively. In addition, EtfA and EtfB from *C. salexigens* also share 74% and 73% similarities with the predicted PA5400 and PA5401 gene products of *P. aeruginosa* PAO1, respectively. Although the gene organization flanking *dgcA* and *dgcB* genes in *P. aeruginosa* PAO1 is similar to that flanking *csal_0990* and *csal_0991* in *C. salexigens* DSM 3043 (Fig. S4), there is no ORF overlap between the three adjacent genes (PA5399, PA5400, and PA5401), and their intergenic DNA lengths are 118 bp and 35 bp, respectively. Moreover, an inverted-repeat sequence was also found immediately downstream of *etfB*, which might function as a transcription terminator of the operon.

Genetic confirmation of the genes involved in DMG degradation to sarcosine. To determine whether the *csal_0990*, *csal_0991*, *csal_0992*, and *csal_0993* genes are involved in the conversion of DMG to sarcosine in *C. salexigens*, four single-gene deletion mutants, designated CSΔ0990, CSΔ0991, CSΔ0992, and CSΔ0993, respectively, were constructed with ZW4-1 as the wild-type strain. In the markerless in-frame deletion mutants CSΔ0991, CSΔ0992, and CSΔ0993, the coding regions of *csal_0991*, *csal_0992*, and *csal_0993* were separately truncated into three ORFs of 36, 126, and 42 bp in length, encoding 11, 41, and 13 amino acid residues, respectively. In the case of CSΔ0990, since for unknown reasons we could not obtain a markerless in-frame deletion mutant, a *csal_0990* mutant that conferred chloramphenicol resistance was constructed. The resultant four mutants lost their ability to grow on S-M63 agar plates using DMG as the sole N source but were still capable of utilizing sarcosine and glycine as the sole N source (data not shown). These findings suggested that the four genes are essential for DMG degradation to sarcosine in *C. salexigens*.

Catabolism of DMG results in release of ammonium. As shown in Fig. 3A, commensalism was observed when strain ZW4-1 and the four mutants (CSΔ0990, CSΔ0991, CSΔ0992, and CSΔ0993) were streaked on the same S-M63 agar plate with DMG as the sole N source. We hypothesized that growth of the mutants on DMG was restored once they could access an exogenous N source released by ZW4-1. The nitrogen-containing compounds are most likely to be sarcosine, glycine, serine, and/or ammonium, since the N atom in DMG is removed in the form of ammonium in the serine deamination reaction (Fig. 1). ^{13}C-NMR and high-pressure liquid chromatography (HPLC) analyses did not reveal the presence of sarcosine, glycine, and/or serine in the culture medium, while an ion chromatography experiment confirmed that the nitrogen-containing substance was ammonium (Fig. 3B). We further investigated the relationship between cell growth and ammonium concentrations in the culture broth. As the concentrations of DMG in the liquid medium gradually decreased due to assimilation by ZW4-1, the concentrations of ammonium increased accordingly (Fig. 3C),

reaching the highest level of 17.8 mM, and then gradually decreased to 9.3 mM. These observations indicated that a large portion of ammonium is first released outside the cells during the process of DMG catabolism and then reabsorbed. Although later the concentration of ammonium in the culture broth slowly increased once again, the reason was probably cell lysis after the cells reached the stationary phase. It should be noted that diauxic growth was observed under these conditions, and a similar phenomenon has previously been reported for cells grown in minimal medium with GB as the sole N source (30).

Complementation of the Δ*csal_0990* mutant. Due to a concern about the potential polar effect of fragment insertion in *csal_0990* on its downstream genes, we complemented the *csal_0990* mutant (CSΔ0990, Rif^rCm^r) with the full length of *csal_0990*, including its putative promoter region, on a broad-host-range vector, pBBR1MCS-2 (Km^r). Since the intergenic sequence between *csal_0989* and *csal_0990* is just 10 bp, the whole promoter region of *csal_0990* is unlikely to be located in this region. The results of operon prediction programs suggested that the six genes (*csal_0988* to *csal_0993*) or five of the six genes (*csal_0989* to *csal_0993*) might form an operon. Therefore, the "long fragment" and the "short fragment" were PCR amplified as described in Materials and Methods and inserted into the broad-host-range vector pBBR1MCS-2 (Fig. S5A). The two complemented strains CSΔ0990(pBBR1MCS2-HBL90) and CSΔ0990(pBBR1MCS2-HBS90) were able to grow in S-M63 with DMG as the sole N source, although their growth rates were significantly lower than that of the wild type, while CSΔ0990(pBBR1MCS2), as a negative control, was still unable to grow in the same medium (Fig. S5B). Moreover, both of these complemented strains also could grow on DMG as the sole C source. However, the lag phases of the mutants were prolonged to 7 to 8 days, and their growth was very poor (optical density at 600 nm [OD_{600}], <0.35). It is noteworthy that this gene is not sufficient for DMG degradation to sarcosine, as growth defects of the other three mutants (CSΔ0991, CSΔ0992, and CSΔ0993) were rescued by neither of the two plasmids.

Overexpression and purification of DddhC. To further investigate the function of DddhC *in vitro*, the *csal_0990* gene was overexpressed in *E. coli* as an N-terminally 6×His-tagged fusion protein (His_6-DddhC) and purified from the soluble protein fraction of *E. coli* using Ni^{2+}-chelating affinity chromatography. Addition of riboflavin to the culture medium increases the supply of flavin and favors production of soluble flavin-containing enzymes in *E. coli*. After optimization, induction with 0.05 mM IPTG (isopropyl-β-D-thiogalactopyranoside) at 25°C for 12 to 15 h produced the maximum level of soluble active enzyme, and the yield was estimated to be approximately 13.8 ± 2.3 mg/liter. On an SDS-PAGE gel, denatured His_6-DddhC had a molecular mass of approximately 77.2 kDa (Fig. S6A), which was close to the value of 78.507 kDa calculated based on its amino acid sequence. The molecular weight of the native His_6-DddhC was estimated to be approximately 7.9×10^4 by gel filtration chromatography (Fig. S6B), suggesting a monomeric structure. Interestingly, we found that the purified enzyme could exist in the form of a monomer, dimer, or polymer under nondenaturing conditions (Fig. S6D), but only the protein in the form of a monomer exhibited enzyme activity. In addition, DddhC was also overexpressed as a C-terminally 6×His-tagged fusion protein with pET28a as the expression vector and *E. coli* BL21(DE3) as the host strain. However, the purified enzyme showed no activity, although the recombinant protein was soluble in the crude extracts of *E. coli*, indicating that addition of His-tag to the C terminus of DddhC can seriously affect enzyme activity.

Spectroscopic properties of DddhC and its flavin content. The purified DddhC-His_6 was colorless, while the His_6-DddhC solution was bright yellow, having a typical absorption spectrum of oxidized flavoprotein, with maxima at 222, 275, 370, and 440 nm and one shoulder at around 470 nm (Fig. 4A). After heat denaturation, the supernatant of the enzyme (His_6-DddhC) solution was yellow, while the protein sediment was white. The UV-visible spectrum of the yellow supernatant showed absorption maxima at 372 and 450 nm (Fig. 4B), which are characteristic properties of flavin, suggesting the presence

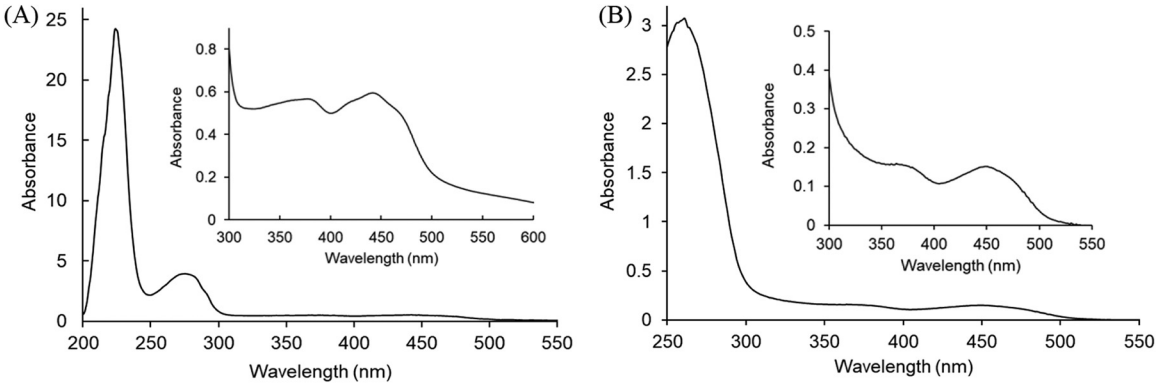

FIG 4 (A and B) UV-visible absorption spectra of purified His6-DdhC (24 μM) (A) and its heat-released flavin (13 μM) (B) in 20 mM PBS buffer (pH 7.5). The insets are the magnified views of the spectra, focusing on the wavelength ranging from 300 to 600 nm.

of a non-covalently bound flavin cofactor in DdhC. The free flavin in the supernatant was identified by HPLC analysis as flavin adenine dinucleotide (FAD) (data not shown) and quantified to be 1.06 $\pm$ 0.08 mol per mole of protein. No fluorescence was observed for the protein sediment after SDS-PAGE separation, suggesting that no flavin cofactor is covalently bound with DdhC.

Catalytic properties of His_6-DdhC. The DMGDH activity of DdhC was measured with the dye-linked assay systems (phenazine methosulfate [PMS]/2,6-dichlorophenol indophenol [DCPIP] or PMS/nitrotetrazolium blue chloride [NBT]). Since the absolute difference of absorbance between experimental group and control group in the PMS/NBT system is about 4 to 6 times that of the PMS/DCPIP system, the former system was routinely employed to measure enzyme activity, except for the kinetic assays with NAD^+ and $NADP^+$ as substrates. No activity band was observed in the absence of either PMS or DMG, indicating that electrons are not directly transferred from DMG to NBT (Fig. S6C), and formation of the active band is substrate specific, not caused by nonspecific adsorption of dyes (Fig. S6C). Given the fact that the amount of formaldehyde measured by the Nash method (10) is much lower than its actual content due to interference by PMS in the reaction mixture, the method described by Colby and Zatman (31) was employed and gave reproducible results. The molar ratio of DMG consumption to the production of sarcosine and formaldehyde was determined to be approximately 1:1:1.

The optimal temperature for purified DdhC was 60°C (Fig. 5A). The enzyme was active over a wide pH range of 4.0 to 11.0, exhibiting maximal activity at pH 7.0 to 8.0 (Fig. 5B). Since the background of the control group increased significantly when the pH value of the buffer was >8.0, 20 mM PBS buffer (pH 7.5) was routinely used in the standard assay mixture (Fig. S7). Interestingly, DdhC showed 64% and 24% of maximal

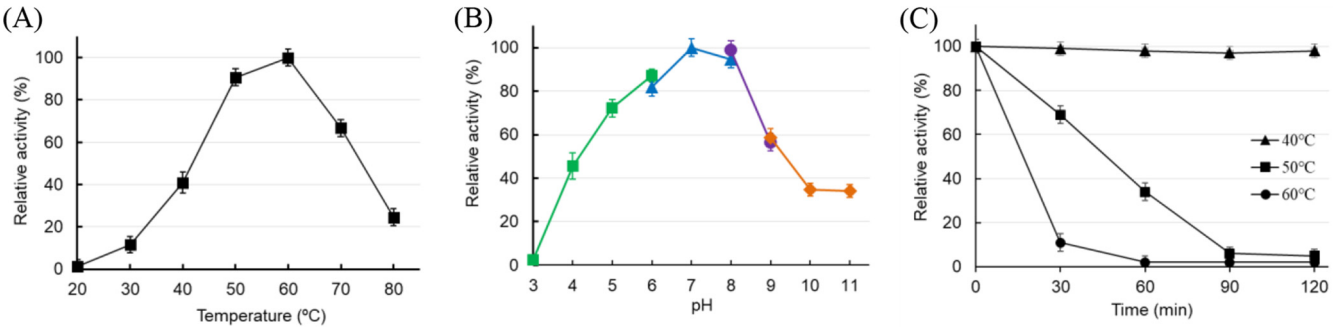

FIG 5 Effects of temperature and pH on the activity of DdhC and its thermostability. (A) Effect of temperature on DMGDH activity. (B) Effect of pH on DMGDH activity. The buffers used include sodium acetate (pH 4.0 to 6.0), PBS (pH 6.0 to 8.0), Tris-HCl (pH 8.0 to 9.0), and glycine-NaOH (pH 9.0 to 11.0). (C) Thermostability of DdhC. All measurements were carried out in triplicate.

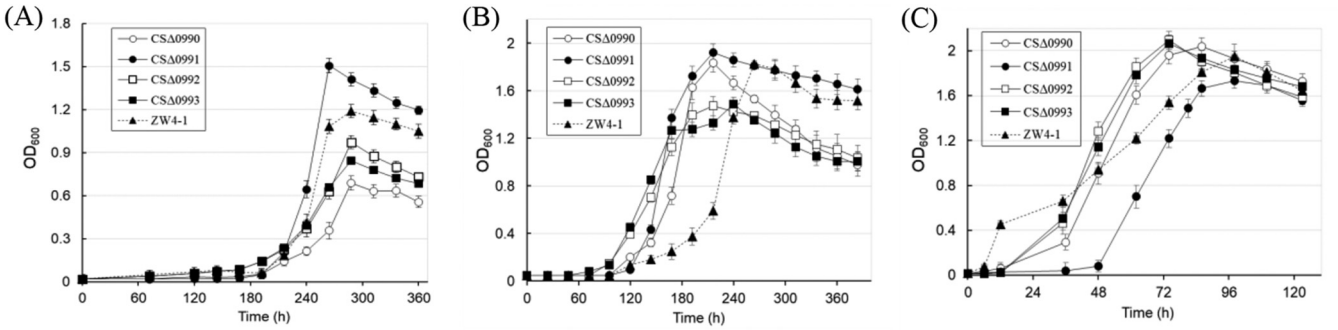

FIG 6 (A to C) Growth of the four DMG$^-$ mutants (CSΔ0990, CSΔ0991, CSΔ0992, and CSΔ0993) in liquid S-M63 medium containing 1 M NaCl with sarcosine as the sole N source in the absence of DMG (A and B) or the presence of 20 mM DMG (C). The cultures were incubated at 37°C (A and C) and 25°C (B).

activity at 70°C and 80°C, respectively, indicating its thermotolerant properties (Fig. 5C). However, the enzyme was only stable at temperatures lower than 40°C and maintained 36% and less than 1% residual activities after incubation for 60 min at 50°C or 60°C, respectively. When stored at −20°C for 1 month in 50% glycerol, the enzyme activity remained almost unchanged. However, the activity decreased to 52% of its original level after incubation at 4°C for 72 h.

The effects of metal ions (Na^+, K^+, Ca^{2+}, Zn^{2+}, Mn^{2+}, Mg^{2+}, Fe^{2+}, and Co^{2+}) and EDTA at a final concentration of 2 mM on the enzyme activity were also examined. DdhC did not need deliberate addition of metal ions to maintain its activity. Among the metal ions tested, Ca^{2+} increased the activity by 12%, while the other metal ions tested had no or slightly inhibitory effects, and EDTA, the chelating agent, inhibited the activity by 33%.

Substrate specificity and steady-state kinetics. The substrate specificity of DdhC was investigated with several methylated amines, such as DMG, sarcosine, GB, choline, histamine, and TMA. The enzyme could use DMG and sarcosine as substrates but did not show activity toward TMA, histamine, GB, or choline. In addition, the enzyme exhibited dual coenzyme specificity, preferring NAD^+ to $NADP^+$. No activity was detected in the absence of NAD^+ or $NADP^+$ with the PMS/DCPIP dye-linked system, indicating that the enzyme is $NAD(P)^+$ dependent.

Kinetic studies of DdhC were performed using the analysis of initial rates with NAD^+, $NADP^+$, DMG, and sarcosine as substrates. The K_m values of DdhC for DMG, sarcosine, NAD^+, and $NADP^+$ were determined to be 8.61 ± 1.43, 14.85 ± 1.64, 0.81 ± 0.16, and 3.21 ± 0.36 mM, respectively, and the V_{max} values were 0.048 ± 0.004, 0.043 ± 0.003, 0.031 ± 0.002, and 0.021 ± 0.001 U mg^{-1} of protein, respectively. The k_{cat} values were 0.312 ± 0.026, 0.280 ± 0.020, 0.202 ± 0.013, and 0.136 ± 0.006 s^{-1}, respectively (Fig. S8).

Addition of DMG greatly improved growth of the four DMG$^-$ mutants at 37°C. When cultured at 37°C in S-M63 containing sarcosine as the sole N source, all of the four mutants (CSΔ0990, CSΔ0991, CSΔ0992, and CSΔ0993) grew very slowly. Among them, CSΔ0991 grew fastest (Fig. 6A). Accidentally, we found that the growth rates and yields of strain ZW4-1 and the mutants grown at 25°C were much higher than those at 37°C (Fig. 6B). Unexpectedly, the growth rates of the four mutants at 37°C were significantly improved (Fig. 6C) after exogenous addition of DMG. Since the DMG catabolic pathway in the mutants has been blocked, the cells cannot utilize DMG as a nutrient. We speculated that the presence of DMG in the growth medium enables the cells to transport and accumulate DMG intracellularly or induces the biosynthesis of other kinds of compatible solutes. To further confirm our hypothesis, a ^{13}C-NMR experiment was performed. When grown at 37°C in S-M63 with sarcosine as the sole N source, ZW4-1 cells accumulated ectoine, hydroxyectoine, glutamate, NADA, and sarcosine (Fig. 7A), while the mutants, in addition to these substances, also accumulated trehalose and GG intracellularly (data not shown). These results indicated that once the catabolic path-

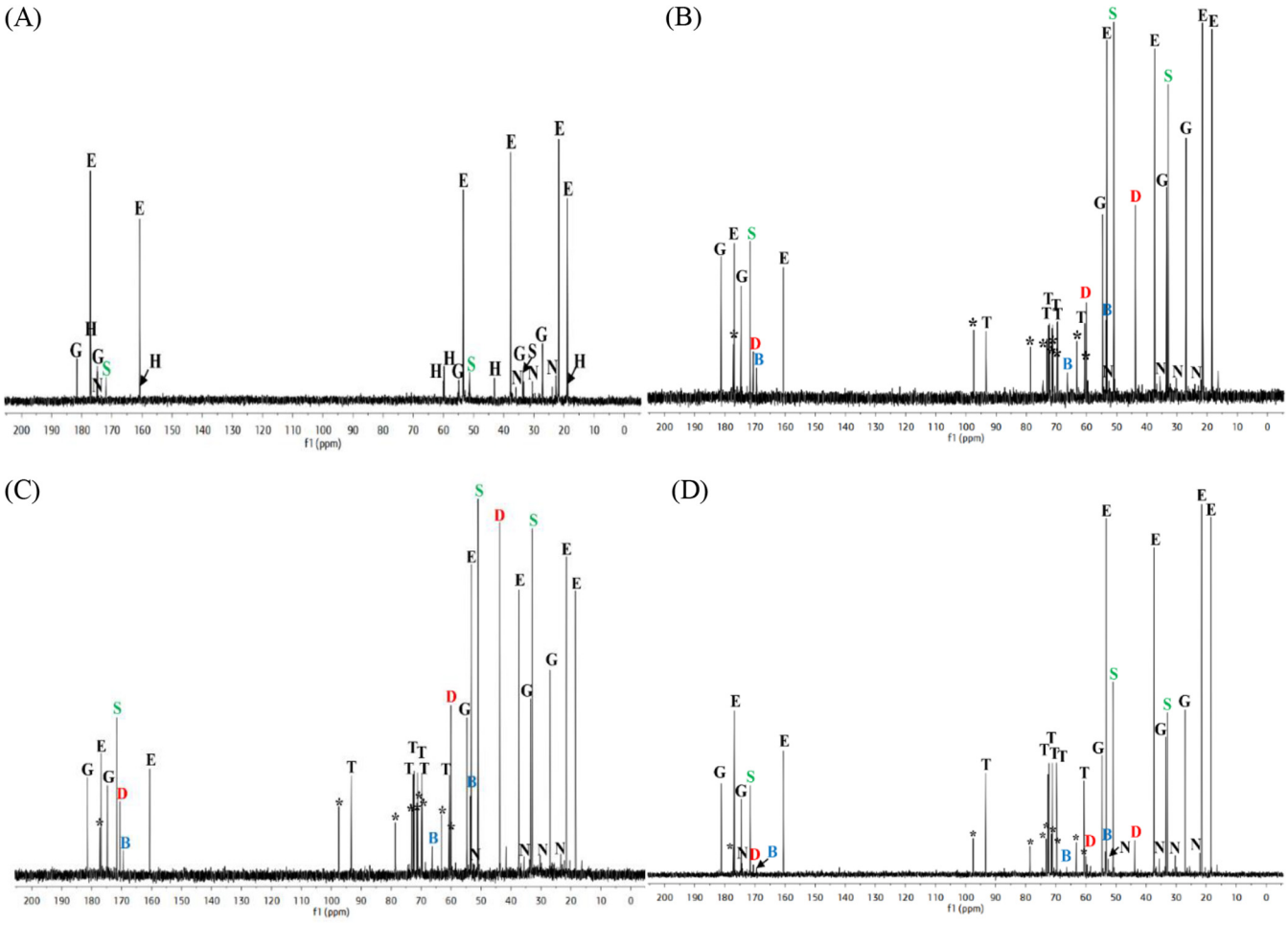

FIG 7 Natural abundance ^{13}C-NMR spectra of major cytosolic solutes of *C. salexigens* ZW4-1 and its mutants. (A) ^{13}C-NMR spectra of major cytosolic solutes of ZW4-1 cells grown in S-M63 plus 1 M NaCl with sarcosine as the sole N source. (B to D) ^{13}C-NMR spectra of major cytosolic solutes of CSΔ0990 (B), CSΔ0991 (C), and CSΔ0993 (D). The signals were as follows: GB (B), DMG (D), sarcosine (S), ectoine (E), hydroxyectoine (H), glutamate (G), NADA (N), trehalose (T), and glucosylglycerate (*).

way of DMG is blocked, the inhibition on biosynthesis of trehalose and GG is relieved. After DMG was added to S-M63 containing sarcosine as the sole N source, the peaks assigned to GB and DMG were detected in cell extracts of the mutants, but the signals of hydroxyectoine disappeared (Fig. 7B to D). In addition, the signal intensities of trehalose and GG were much higher than those without addition of DMG. Therefore, the improvement of thermotolerance for these mutants is probably due to combined effects of these compatible solutes, including GB and DMG accumulated intracellularly.

DISCUSSION

Mechanism of the reaction catalyzed by DdhC. As early as the late 1980s, Smith et al. first described the presence of DMGDH activity in cell extracts of *S. meliloti* (1). Later, Wargo et al. found that *dgcA* and *dgcB* in *P. aeruginosa* PAO1 are involved in DMG catabolism to sarcosine (26). In this study, the *csal_0990* gene product (DdhC) from *C. salexigens* DSM 3043, which shares homology with the predicted *dgcA* product, was proved to be a novel NAD(P)$^+$-dependent, FAD-containing DMGDH, catalyzing the oxidative *N*-demethylation of DMG with the formation of stoichiometric quantities of sarcosine and formaldehyde. For a flavoprotein, the flavin moiety is always the hydrogen acceptor in oxidation reactions that remove two hydrogen atoms from a substrate, since the free-energy change is insufficient to reduce NAD(P)$^+$. The flavin cofactor accepts electrons from the reducing substrate and then transfers the electrons to other

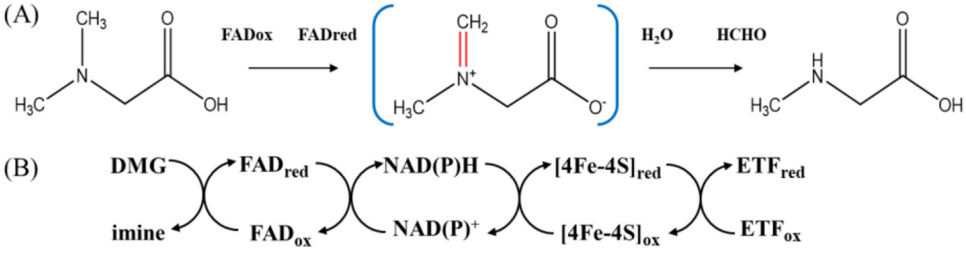

FIG 8 Proposed reaction mechanism of the DdhC-catalyzed conversion of DMG to sarcosine in *C. salexigens* DSM 3043. (A) Oxidation of DMG is accompanied by the reduction of FAD. A hypothetical intermediate (brackets) was hydrolyzed in the presence of water, producing sarcosine and formaldehyde. (B) Proposed sequence of oxidation-reduction reactions in the conversion of DMG to sarcosine. Abbreviations or symbols: FADox, [4Fe-4S]ox, and ETFox represent the oxidized forms of FAD, 4Fe-4S center, and ETF, respectively; FADred, [4Fe-4S]red, and ETFred represent the reduced forms of FAD, [4Fe-4S] center, and ETF, respectively.

electron acceptors (32). Based on the reaction products, a possible reaction mechanism of DdhC toward DMG was proposed (Fig. 8). The C-N bond in DMG is oxidized with DdhC by removal of a hydride equivalent to form a labile imine intermediate. Subsequently, the imine intermediate is spontaneously hydrolyzed in the presence of water, producing sarcosine and formaldehyde (Fig. 8A). On the other hand, the two protons subtracted from DMG (one from the carbon and another from the positively charged nitrogen) are transferred to the non-covalently bound FAD, resulting in the reduced form of FAD, which is subsequently reoxidized by coupling with reduction of the enzyme-bound $NAD(P)^+$. Regeneration of $NAD(P)^+$ is achieved by electron transfer to the [4Fe-4S] cluster in the putative membrane-anchored ferredoxin (the *csal_0991* gene product), which in turn transfers the electrons to the oxidized heterodimeric flavoprotein ETF (the *csal_0992* and *csal_0993* gene products) for further utilization in the membrane respiratory chain (Fig. 8B). The overall electron flow can be summarized as follows: DMG → DMGDH → ferredoxin → ETF.

It should be noted that DdhC is a flavoenzyme and does not contain any [4Fe-4S] clusters, while TMA dehydrogenase (TMADH) from *Methylophilus methylotrophus*, dimethylamine dehydrogenase (DMADH) from *Hyphomicrobium* sp. X, and histamine dehydrogenase (HADH) from *Nocardioides simplex*, as amine-oxidizing dehydrogenases, are [4Fe-4S] cluster-containing iron-sulfur flavoenzymes, all of which use ETF as the physiological electron acceptor. Although the [4Fe-4S] cluster is absent in DdhC, the *csal_0991* gene product was predicted to be a ferredoxin containing two [4Fe-4S] clusters (33, 34). In some iron-sulfur flavoproteins, the iron-sulfur-binding domain can exist as either a separate protein or a domain linked in different combinations to flavin and pyridine nucleotide-binding domains (35). Therefore, it is likely that the predicted ferredoxin serves the same function as the [4Fe-4S] clusters of the three amine-oxidizing dehydrogenases in transferring electrons from DMGDH to ETF.

Most of the ETFs characterized so far are heterodimers composed of α and β subunits and play an important role in the β-oxidation of fatty acids and some oxidative demethylation reactions by coupling several flavoprotein dehydrogenases to the electron transport chain (36). In the mammalian mitochondrial matrix, DMGDH is reoxidized by ETF. Subsequently, the membrane-bound ETF ubiquinone oxidoreductase (ETF-QO) accepts electrons from ETF and efficiently transfers these electrons to the ubiquinone pool of the respiratory redox chain in mitochondria (37). For *C. salexigens*, two sets of ETF-encoding genes (*csal_0992-csal_0993* and *csal_1614-csal_1613*) have been identified in its genome. The amino acid sequence identities between the two α subunits and the two β subunits of ETFs were 19.7% and 14.5%, respectively. In this study, gene disruption experiments showed that the Δ*csal_0992* and Δ*csal_0993* mutants lost their abilities to grow on DMG, indicating that the ETF encoded by *csal_0992-csal_0993* participates in the electron transfer process during DMG degradation to sarcosine, while the other ETF does not. Moreover, a BLAST search revealed the presence of an ETF-QO homolog (the predicted *csal_1612* product) in *C. salexigens* that shares 54.23%

amino acid sequence identity with the ETF-QO from *Rhodobacter sphaeroides* (38). It seems likely that the ETF and ETF-QO link DMG oxidation to the membrane respiratory system. However, we failed to obtain the Δ*csal_1612* mutant, probably because the mutation is lethal to the cells. The exact role of the *csal_1612* gene product in the DMG catabolic pathway needs to be further experimentally determined.

Conserved-domain analysis of DdhC. Among the available proteins deposited in the Protein Data Bank (PDB), the 2,4-dienoyl-CoA reductase (DCR) from *E. coli* is an iron-sulfur flavoprotein and shows the highest sequence similarity (46.9%) to DdhC (39). Based on the structure of *E. coli* DCR, the whole polypeptide chain of DdhC can be segregated into four segments and comprises three domains. The first segment (residues 1 to 385) forms the large domain at the N terminus of the polypeptide. The medium domain is made up of the second (residues 386 to 486) and fourth (residues 621 to 692) fragments. The third fragment (residues 487 to 620), which lies in the medium domain, forms the small domain. A conserved sequence motif [(V/I)$GX_{1\text{-}2}$GXXGXXX(G/A), where X is any other amino acid (Fig. S9)] that binds FAD or NAD(P)H in the Rossman fold is located in the second fragment (27). The large domain contains an aldolase-type triose phosphate isomerase (TIM) barrel fold and is homologous to a large group of flavin mononucleotide (FMN)-containing proteins called old yellow enzymes (OYEs), belonging to the NADH:flavin oxidoreductase/NADH oxidase (Oxidored_FMN) family (pfam00724), while the medium and small domains are rich in α/β structure containing the characteristic dinucleotide-binding motifs, belonging to the pyridine nucleotide-disulfide oxidoreductase (Pyr_redox_2) family (pfam07992) (40). A common feature of the members of the Pyr_redox_2 family is that a small NAD(P)H-binding domain is located in a larger FAD-binding domain. The topologies of the medium and small domains of DdhC are remarkably similar to the FAD- and NADPH-binding domains of glutathione reductase (GR) (41). Therefore, it is likely that the medium and small domains of DdhC are responsible for binding FAD and NAD(P)H. In addition, the conserved cysteine that has been shown to cross-link with FMN to form 6-*S*-cysteinyl flavin in TMADH (Cys^{30}) (42), DMADH (Cys^{30}) (43), and HADH (Cys^{35}) (44) is absent in DdhC, which may explain why DdhC lacks FMN (Fig. S9). Similar to *E. coli* DCR, evolution of DdhC may be due to the fusion of ancestral genes encoding primitive forms of OYE and GR.

As amine-oxidizing dehydrogenases, both HADH from *N. simplex* (45) and TMADH from *M. methylotrophus* (42, 46) are homodimers, with each subunit containing a covalently linked 6-*S*-cysteinyl FMN and a [4Fe-4S] cluster as redox cofactors at the N-terminal region and a tightly bound ADP of unknown function at the C-terminal region. Although sequence identities between DdhC and the two proteins are very low (~27%), they have similar domain arrangements. However, both HADH and TMADH are iron-sulfur flavoproteins, and the conserved motif (CX_2CX_2C, where X represents any amino acid residue) involved in binding the [4Fe-4S] cluster is located in the large domain of the two proteins (45, 46). As for DdhC, sequence alignment indicated that two of the three conserved cysteine residues are conserved, but the second cysteine is replaced by an alanine (Fig. S9). Netz et al. previously reported that the mutation in the cysteine residue of the conserved motif can severely affect the binding of enzymes to the [4Fe-4S] cluster (47). To further investigate whether the codon replacement at this site occurs only in DdhC, 126 DdhC homologs from members of nine orders, *Pseudomonadales*, *Oceanospirillales*, *Burkholderiales*, *Vibrionales*, *Alteromonadales*, *Rhizobiales*, *Chromatiales*, *Salinisphaerales*, and *Rhodospirillales*, which share more than 52% sequence identity with DdhC were retrieved from the UniProKB/Swiss-Prot database (Fig. S10). Sequence alignments revealed that the alanine residue in the motif is fully conserved in all tested DdhC homologs (data not shown). Although the alanine residue of the conserved motif varies in the other DdhC homologs whose sequence identities are below 52%, the results of genome analysis showed that those microbial cells actually do not contain the DMG degradation pathway. Since DdhC also shares amino acid sequence homology (query coverage, >90%) with the enzymes putative

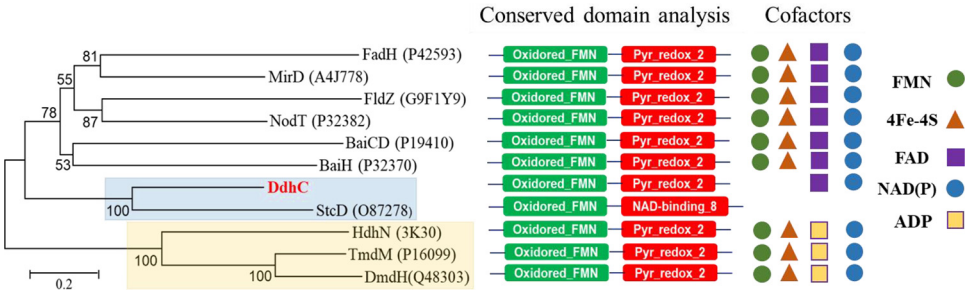

FIG 9 Phylogenetic analysis of DdhC and its homologous proteins. Multiple alignment was performed using Clustal Omega with default parameters. The tree was constructed using the neighbor-joining method in the program MEGA X with the parameters set as described in Materials and Methods. Bootstrap values were calculated from 1,000 repeats, and those greater than or equal to 50% are shown. The scale bar represents two substitutions per 10 amino acids. The UniProt accession numbers of these proteins are indicated in parentheses. Abbreviations: FadH, 2,4-dienoyl-CoA reductase from *E. coli*; MirD, metal reductase from *Desulfotomaculum reducens* MI-1; FldZ, cinnamate reductase from *C. sporogenes* DSM 767; NodT, NADH oxidase from *Thermoanaerobacter brockii*; BaiCD, 3-oxocholoyl-CoA 4-desaturase from *Clostridium scindens* JCM 10418; BaiH, 7-beta-hydroxy-3-oxochol-24-oyl-CoA 4-desaturase from *C. scindens* JCM 10418; StcD, putative *N*-methylproline demethylase from *S. meliloti* strain 1021; HdhN, histamine dehydrogenase from *Nocardioides simplex*; TmdM, trimethylamine dehydrogenase from *Methylophilus methylotrophus* W3A1; DmdH, dimethylamine dehydrogenase from *Hyphomicrobium* sp. X.

N-methylproline demethylase from *S. meliloti* strain 1021 (43.6% identity/59.7% similarity) (48), NADH oxidase from *Thermoanaerobacter brockii* (35.9%/53.3%) (49), metal reductase from *Desulfotomaculum reducens* MI-1 (31.8%/48.6%) (50), 2,4-dienoyl-CoA reductase (DCR) from *E. coli* (29.8%/46.9%,) (39), 3-oxocholoyl-CoA 4-desaturase (EC 1.3.1.115) from *Clostridium scindens* JCM 10418 (31.9%/49.3%) (51), 7-beta-hydroxy-3-oxochol-24-oyl-CoA 4-desaturase (EC 1.3.1.116) from *C. scindens* JCM 10418 (33.7%/50.3%) (51), cinnamate reductase from *Clostridium sporogenes* DSM 767 (30.8%/46.4%) (52), HADH from *N. simplex* (27.22%/43.76%) (45), TMADH (EC 1.5.8.2) from *M. methylotrophus* W3A1 (26.7%/42.1%) (42), and dimethylamine dehydrogenase (DMADH, EC 1.5.8.1) from *Hyphomicrobium* sp. X (25.9%/43.1%) (43), it is not surprising that those DdhC homologs may serve as enzymes with functions different from that of DMGDH, and the conserved sequence motif (CX_2AX_2C, where X represents any amino acid residue) might be used to distinguish DMGDH from closely related protein homologs with different functions.

Phylogenetic analysis of DdhC. Based on its biochemical and spectral properties, DdhC is a novel DMGDH belonging to the family of oxidoreductases that specifically act on the CH-NH group of donors. The amine-oxidizing flavoproteins whose functions have been biochemically characterized constitute a large superfamily of flavin-dependent oxidoreductases, all of which are capable of oxidizing the C-N bond with a wide range of substrate specificities. The superfamily is further classified into three major families: the D-amino acid oxidase/sarcosine oxidase family, the monoamine oxidase family, and the TMADH family (53). Undoubtedly, DdhC belongs to the TMADH family since it shows amino acid sequence similarity to TMADH from *M. methylotrophus* W3A1 (42). However, phylogenetic analysis revealed that DdhC and a putative *N*-methylproline demethylase from *S. meliloti* (48) form a separate group (Fig. 9), which separates them from the other three amine-oxidizing dehydrogenases (TMADH, DMADH, and HADH). Since the amino acid sequence similarities between the members of these two groups are less than 50%, the TMADH family should be upgraded to the TMADH superfamily. Thus, the group containing TMADH, DMADH, and HADH can be renamed the TMADH family, while another group containing DdhC can be renamed the DMGDH family.

Comparison of different types of DMG *N*-demethylating enzymes. Although both *C. salexigens* and mammalian DMGDHs are monomers and functionally similar flavoenzymes with FAD as their cofactors, sequence alignment and biochemical characterization revealed that they are distinct from each other. First, sequence analysis of the DMGDHs from human (17) and rat (54) showed that the two proteins share 90.42%

identity. In contrast, a comparison of the amino acid sequence of *C. salexigens* DMGDH with those of mammalian DMGDHs did not reveal any general similarity. These findings suggested that they are structurally unrelated proteins and might have evolved from distinct ancestral genes. Second, FAD is covalently attached to the apoenzyme of mammalian DMGDH via an 8α-carbon (FAD)/N_3-His linkage (55) and serves as the hydrogen acceptor from DMG, while the flavin is non-covalently bound in DdhC, and the enzyme activity depends on the presence of NAD(P)$^+$. Third, each of the mammalian DMGDHs contains a tetrahydrofolic acid (THF)-binding domain and utilizes a non-covalently bound folate as a coenzyme *in vivo* (56), transferring the detached methyl group to THF to produce 5,10-methylene-THF, termed "active formaldehyde," and preventing accumulation of cell-toxic formaldehyde (54, 55); no conserved THF-binding domain(s) is found in DdhC based on the primary and secondary structure analysis, and the reaction product is formaldehyde rather than active formaldehyde. However, in the absence of THF or *in vitro* assays, the methyl groups from DMG can also be converted to formaldehyde in the reactions catalyzed by the mammalian DMGDHs (17).

Another type of DMG *N*-demethylating enzyme, the DMGO from *A. globiformis*, is a bifunctional enzyme catalyzing the oxidation of DMG, and formation of 5,10-methylene tetrahydrofolate or formaldehyde depends on the availability of THF (57). Interestingly, the enzyme shares ~30% sequence identity with human and rat DMGDHs but has no general sequence similarity to DdhC. The N-terminal region of DMGO binds FAD covalently, while its C-terminal region binds tetrahydrofolate (57). FAD serves as a coenzyme by passing electrons from DMG to its physiological electron acceptor ETF, while THF receives the methyl groups that are removed by DMGO, forming sarcosine and 5,10-methylene-THF. In the databases of some bioinformatics websites, such as NCBI and EMBL, the genes showing amino acid sequence similarities to DMGO from *A. globiformis* should be annotated as microbial DMGOs rather than microbial DMGDHs.

In this study, the k_{cat} value of DdhC toward DMG was determined to be 0.312 ± 0.026 s^{-1}, which seemed to be too low compared with that of DMG oxidase from *A. globiformis* (14.3 s^{-1}) (12). We determined that this might be the result of utilization of an artificial electron intermediator (PMS) and acceptor (NBT or DCPIP) in the DMGDH activity assay. Previously, the apparent first-order rate constant of purified DMGDH from rat liver for DMG was determined to be 0.084 s^{-1} with PMS and DCPIP as the artificial electron intermediator and acceptor, respectively (58).

Ecological significance of releasing ammonium during DMG catabolism. So far, aerobic bacteria can be roughly divided into three types based on the way they accumulate and utilize GB. The first type of bacteria, represented by *E. coli* and *B. subtilis*, accumulate GB intracellularly by uptake from the extracellular environment via the specific transporters that are either induced or activated in hyperosmotic environments (59) or by the endogenous choline-to-GB oxidation pathway. The second type, represented by some halophilic phototrophic eubacteria and methanogens, synthesize GB *de novo* from glycine or take up GB when it is externally available (60–62). Although both types of bacteria accumulate GB as a compatible solute, they cannot use it as a nutrient. Therefore, it is not surprising that the intracellularly accumulated GB has to be released outside the cells when the external osmotic pressure decreases. In view of cellular energy utilization, it is not cost-effective to release endogenously synthesized compatible solutes since synthesis of GB requires consumption of a large amount of reducing equivalents and energy. The third type, such as some species in the genera *Chromohalobacter* and *Pseudomonas* (3) and other GB-catabolizing microorganisms (1), not only can accumulate GB intracellularly as a compatible solute but also can utilize it as a nutrient. In this study, we found that in *C. salexigens*, ammonium is produced and released into the growth medium during the process of DMG catabolism and then reabsorbed by the cells. Thus, it can be expected that the GB released by the first two types of bacteria could be absorbed and degraded by the third type of bacteria to release ammonium under natural conditions. In this way, the first two types of bacteria

indirectly realize the utilization of GB as a nitrogen source, which is ecologically important for increasing bacterial adaptation, considering that many environments are often limited by the availability of inorganic nitrogen.

DMG induces intracellular accumulation of trehalose, GB, and DMG in *C. salexigens*. Trehalose, known as a universal stress molecule found in many prokaryotic and eukaryotic microorganisms, can be synthesized via a two-step enzymatic reaction by trehalose-6-phosphate synthase and trehalose-6-phosphate phosphatase in *C. salexigens*. Accumulation of trehalose in *C. salexigens* has been reported to occur at high temperatures (45°C) in the wild type (23) or at 37°C in the mutants whose ectoine biosynthetic pathway were blocked (25, 63). Trehalose was detected in the intracellular compatible solute pool of ZW4-1 cells grown at 37°C in minimal medium containing DMG (Fig. 2B), but not in the cells grown in minimal medium without addition of DMG (25), suggesting that the presence of DMG induces trehalose production in the wild type. In *C. salexigens*, cytoplasmic accumulation of compatible solutes is highly hierarchical and precisely adjusted to deal with fluctuations in the osmolarity of the growth medium. Cells preferentially accumulate GB through transport from external medium or biosynthesis from choline when these substances are externally available, while endogenous biosynthesis of ectoine and hydroxyectoine is completely or almost completely abolished under these conditions (25). In this study, GB, together with other compatible solutes, was detected in cell extracts of the mutants grown on sarcosine as the sole N source and DMG as an exogenous additive. These findings indicated that the regulatory mechanism of GB biosynthesis from DMG is different from that of GB accumulation and catabolism. Moreover, the presence of GB in the four mutants suggested that the cells could synthesize GB from DMG. It is known that the sarcosine DMG methyltransferases (SDMT, EC 2.1.1.157) found in several halophilic phototrophic eubacteria and methanogens (62, 64) can catalyze the conversion of DMG to GB. However, no SDMT homolog was found in the genome of *C. salexigens* DSM 3043. Therefore, a biochemically unidentified methyltransferase must be present in the cells to catalyze the reaction.

MATERIALS AND METHODS

Chemical reagents. GB, DMG, sarcosine, NAD^+, $NADP^+$, flavin mononucleotide (FMN), and flavin adenine dinucleotide (FAD) were purchased from Sigma-Aldrich (Shanghai, China). DMG hydrochloride, glycine, choline, Ni-nitrilotriacetic acid (NTA) Sefinose resin, phenylhydrazine hydrochloride, phenazine methosulfate (PMS), nitrotetrazolium blue chloride (NBT), 2,6-dichlorophenol indophenol (DCPIP), and isopropyl β-D-thiogalactoside (IPTG) were purchased from Sangon Biotech (Shanghai, China). Trimethylamine and potassium ferricyanide were purchased from Aladdin Bio-Chem Tech (Shanghai, China). All other chemical reagents were commercially available.

Bacterial strains, plasmids, and growth conditions. The bacterial strains and plasmids used in this study are listed in Table 1. All *C. salexigens* strains were routinely grown aerobically at 37°C on D6 agar plates containing (per liter) 58 g NaCl, 5 g $MgSO_4 \cdot 7H_2O$, 5 g tryptone, 5 g yeast extract, and 18 g agar; the pH was adjusted to 7.5 with 2 M KOH. For all growth and complementation experiments, wild-type and mutant strains of *C. salexigens* were grown in S-M63 medium [per liter: NaCl, 58 g; KOH, 4.2 g; KH_2PO_4, 13.6 g; $MgSO_4$, 0.12 g; $FeSO_4 \cdot 7H_2O$, 4.0 mg; $(NH_4)_2SO_4$, 2 g; and D-glucose, 3.6 g; the pH was adjusted to 7.5 using 10 M NaOH]. *Escherichia coli* DH5α and S17-1, used for cloning and conjugation purposes, respectively, were routinely grown in Luria-Bertani medium (65). Both *C. salexigens* and *E. coli* cells were incubated aerobically at 37°C with shaking (120 rpm) on a rotary shaker unless otherwise specified. In the nitrogen-utilizing experiments, ammonia sulfate in the standard S-M63 recipe was replaced with GB, DMG, sarcosine, or glycine at a final concentration of 20 mM. In the carbon-utilizing experiments, glucose was replaced with GB, DMG, sarcosine, or glycine at a final concentration of 20 mM. When required, antibiotics were added to the medium at the final concentrations of 70 $\mu g \cdot ml^{-1}$ chloramphenicol (Cm), 50 $\mu g \cdot ml^{-1}$ kanamycin (Km), and 50 $\mu g \cdot ml^{-1}$ rifampin (Rif). Growth was recorded by measuring the optical density at 600 nm (OD_{600}) with a UV230II UV-visible spectrophotometer (Techcomp, Shanghai, China).

DNA manipulation and PCR. General DNA manipulation was performed according to standard protocols (65). Extraction of bacterial DNA, isolation of plasmid DNA, and purification of PCR-amplified DNA fragments were performed with the FastPure bacterial DNA isolation minikit, FastPure plasmid minikit, and FastPure gel DNA extraction minikit (Vazyme, China), respectively. Restriction endonucleases and T_4 DNA ligase, purchased from TaKaRa Biotech (Dalian, China), were used as recommended by the manufacturer's instructions. Colony PCR was performed as described previously (24). The primers used for PCR amplification are listed in Table 2.

Extraction of intracellular solutes and ^{13}C-NMR analysis. Cells were harvested by centrifugation and washed twice with the carbon-free growth medium. Intracellular solutes were extracted using the

TABLE 1 Bacterial strains and plasmids used in this study

Strain or plasmid	Genotype or description[a]	Source or reference
Strains		
C. salexigens strain DSM 3043	Wild type	DSMZ[b]
ZW4-1	A spontaneous rifampin-resistant mutant of *C. salexigens* DSM 3043	24
CSΔ0990	*csal_0990* deletion mutant of strain ZW4-1, Rif^r Cm^r	This study
CSΔ0991	*csal_0991* in-frame deletion mutant of strain ZW4-1, Rif^r	This study
CSΔ0992	*csal_0992* in-frame deletion mutant of strain ZW4-1, Rif^r	This study
CSΔ0993	*csal_0993* in-frame deletion mutant of strain ZW4-1, Rif^r	This study
E. coli strains		
E. coli DH5α	*supE44* Δ*lacU169* (Φ80*lacZ* M15) *hsdR17 recA1 endA1 gyrA96 thi-1 relA1*	TaKaRa
E. coli S17-1 *λpir*	*pro hsdR recA* RP4-2 (Tc::Mu)(Km::Tn7) (*λpir*)	10
E. coli BL21(DE3)	F$^-$ *ompT hsdS*$_B$(r_B^- m_B^-) *gal dcm* (DE3); T7 RNA polymerase gene under the control of the *lacUV* promoter	TianGen
Plasmids		
pK18mobsacB	Km^r, *mob sacB* (RP4) *lacZ*	10
pK18mobsacB::Δ0990::cat	pK18mobsacB carrying truncated *csal_0990* gene	This study
pK18mobsacB::Δ0991	pK18mobsacB carrying truncated *csal_0991* gene	This study
pK18mobsacB::Δ0992	pK18mobsacB carrying truncated *csal_0992* gene	This study
pK18mobsacB::Δ0993	pK18mobsacB carrying truncated *csal_0993* gene	This study
pBBR1MCS-2	Broad-host-range vector, Km^r	68
pBBR1MCS2-HBL90	pBBR1MCS-2 carrying the "long fragment," Km^r	This study
pBBR1MCS2-HBS90	pBBR1MCS-2 carrying the "short fragment," Km^r	This study
pET-28a(+)	T7 promoter expression vector, Km^r	Novagen
pET28-N0990	pET28a carrying *ddhC (csal_0990)* under the control of the T7 promoter with 6×His-tag added at the N terminus of the fusion protein (His_6-DdhC)	This study

[a]Rif^r, rifampin resistance; Cm^r, chloramphenicol resistance; Km^r, kanamycin resistance.
[b]DSMZ, German Collection of Microorganisms and Cell Cultures.

method described by García-Estepa et al. (23), and then freeze-dried extracts were dissolved in 0.5 ml of D_2O. Natural abundance ^{13}C-NMR spectra were measured at 25°C with a Bruker Advance III high-definition (HD) 500-MHz superconducting Fourier transform (FT) NMR spectrometer. ^{13}C-NMR chemical shifts were referenced to an external dimethyl sulfoxide standard (δ = 40.6 ppm), and the type of compatible solute was identified by comparison of ^{13}C-NMR spectra with corresponding spectra of authentic samples measured under the same conditions or with previously published chemical shift values (66).

Gene deletion and complementation assays. The *csal0990*, *csal0991*, *csal0992*, and *csal0993* single-gene deletion mutants of strain ZW4-1 were constructed using allele exchange with suicide vector pK18mobsacB (24). Briefly, the ~1-kb up- and downstream flanking regions of the target genes were PCR amplified from the genomic DNA of *C. salexigens* ZW4-1 using the primer sets listed in Table 2. For construction of the Δ*csal_0990* mutant, the two amplicons were digested with EcoRI/BamHI and BamHI/HindIII, respectively, and inserted into the EcoRI-HindIII sites of pK18mobsacB, yielding pK18mobsacB::Δ0990. Then, a chloramphenicol (Cm) resistance cassette (1,036 bp) was amplified from plasmid pACYCDuet1 with the primers cat-F and cat-R, digested with BamHI, and inserted into the BamHI site of pK18mobsacB::Δ0990, creating pK18mobsacB::Δ0990::cat, in which part of the *csal_0990* (1,839 bp) gene is replaced by the Cm resistance cassette (1,036 bp). For construction of the Δ*csal_0991*, Δ*csal_0992*, and Δ*csal_0993* mutants, the two amplicons of each target gene were fused together by splicing by overlapping extension PCR (SOE-PCR) (67) and inserted into the EcoRI-HindIII sites of pK18mobsacB using the ClonExpress MultiS one-step cloning kit (Vazyme, China). The resultant knockout vector pK18mobsacB::Δ0991 contained the mutant allele of *csal_0991* with an internal 1,977-bp deletion, and pK18mobsacB::Δ0992 contained the mutant allele of *csal_0992* with an internal 1,143-bp deletion, while pK18mobsacB::Δ0993 contained the mutant allele of *csal_0993* with an internal 762-bp deletion. Then, the knockout vectors were transformed into *E. coli* S17-1 cells, which subsequently passed the vector into strain ZW4-1 by biparental mating. Single-crossover and double-crossover mutants were screened as described previously (10), and the deletion mutants were verified using colony PCR and DNA sequencing.

To complement the Δ*csal_0990* mutant (strain CSΔ0990) with a functional *ddhC* gene on vector pBBR1MCS-2 (68), two DNA fragments containing the coding region of the *csal_0990* gene with its potentially native promoter region were amplified from the genomic DNA of *C. salexigens*. One fragment (the "long fragment") comprised 3,987 bp and contained the region from the first nucleotide downstream of the *csal_0987* termination codon to the last nucleotide of the *csal_0990* termination codon, while the other fragment (the "short fragment") comprised 2,811 bp and contained the region from the first nucleotide downstream of the *csal_0988* termination codon to the last nucleotide of the *csal_0990* termination codon. The resulting amplicons were individually gel purified, digested with EcoRI and BamHI, and then inserted into pBBR1MCS-2 previously linearized with the same enzymes, creating pBBR1MCS2-HBL90 (containing the "long fragment") and pBBR1MCS2-HBS90 (containing the "short fragment"), respectively. The insertions in the recombinant vectors were confirmed by resequencing.

TABLE 2 Primers used in this study

Primer	Sequence (from 5′ to 3′)[a]	Purpose
0990uF	CCGGAATTCAAAGAGGTATGGGGCGC (EcoRI)	Amplification of upstream flanking region of *csal_0990* for construction of pK18mobsacB::Δ0990
0990uR	CGCGGATCCGCGTATGGTGAGATTGCC (BamHI)	
0990dF	CGCGGATCCAAGGATCAGTCGCGCAA (BamHI)	Amplification of downstream flanking region of *csal_0990* for construction of pK18mobsacB::Δ0990
0990dR	ACCCAAGCTTCATCAGACTCTTGGGCAAAC (HindIII)	
cat-F	CGCGGATCCTGTCCGGCGGTGCTTTTGCC (BamHI)	Amplification of chloramphenicol resistance cassette from plasmid pACYCDuet1
cat-R	CGCGGATCCTTACGCCCCGCCCTGCCACT (BamHI)	
0991uF	**tatgaccatgattac**AAGCGCAAGGTAGTGGTG	Amplification of upstream flanking region of *csal_0991* for construction of pK18mobsacB::Δ0991
0991uR	**gcacctcctc**CAGGAGGATATCGAGCATGTC	
0991dF	**tatcctcctg**GAGGAGGTGCTGTCATGAGT	Amplification of downstream flanking region of *csal_0991* for construction of pK18mobsacB::Δ0991
0991dR	**acgacggccagtgcc**ATGCCCACTGCGATGTAGA	
0992uF	**tatgaccatgattac**AAGAAACTGGTGCAGGACATG	Amplification of upstream flanking region of *csal_0992* for construction of pK18mobsacB::Δ0992
0992uR	**gggtcgaatc**ATTGCGGGCGATCCATTC	
0992dF	**cgcccgcaat**GATTCGACCCAGATACTC	Amplification of downstream flanking region of *csal_0992* for construction of pK18mobsacB::Δ0992
0992dR	**acgacggccagtgcc**TCGTCCGGTATTGATGGTC	
0993uF	**tatgaccatgattac**CACAAGCCATTGACCGAGATC	Amplification of upstream flanking region of *csal_0993* for construction of pK18mobsacB::Δ0993
0993uR	**cttcttcgtc**CATGGCAGATTCAGGCTGCAT	
0993dF	**atctgccatg**GACGAAGAAGTACTGCGTTGA	Amplification of downstream flanking region of *csal_0993* for construction of pK18mobsacB::Δ0993
0993dR	**acgacggccagtgcc**GATCTCGCTCAATCTCTCGGT	
sacB-F	CGACAACCATACGCTGAGAG	Amplification of partial *sacB* gene fragment
sacB-R	CGAAGCCCAACCTTTCATA	
0990-test-F	CGGTCTGCTATTCCCATT	Primers for screening of *csal_0990* double-crossover mutant strains
0990-test-R	TTGCGCGACTGATCCTT	
0991-test-F	TCTATTACGCCCTCAAGGAT	Primers for screening of *csal_0991* double-crossover mutant strains
0991-test-R	GGTGATAGGCGTCCCAAT	
0992-test-F	TGCTCAAGAACGAATACGG	Primers for screening of *csal_0992* double-crossover mutant strains
0992-test-R	CGCCCATTCATCGTCATT	
0993-test-F	ATTGGGACGCCTATCACC	Primers for screening of *csal_0993* double-crossover mutant strains
0993-test-R	GTCGTCCGGTATTGATGGT	
0990HBLF	**gataagcttgatatc**AGTCTCGCACTCCCGCCGCTT	Amplification of the "long fragment" for construction of pBBR1MCS2-HBL90
0990HBLR	**cgctctagaactagt**TCAGAAGTCCTTGCAGATCCGCAG	
0990HBSF	**gataagcttgatatc**GGGCAATACTTCTGCATATAAGG	Amplification of the "short fragment" for construction of pBBR1MCS2-HBS90
0990HBSR	**cgctctagaactagt**TCAGAAGTCCTTGCAGATCC	
N0990F	CGCCATATGGCATTCGATGCGTTG (NdeI)	Amplification of the *ddhC* (*csal_0990*) gene for construction of pET28a-N0990
N0990R	CCCAAGCTTTCAGAAGTCCTTGCAGATCCG (HindIII)	

[a]Sequences in bold lowercase letters are the plasmid sequences used for homologous recombination. Restriction sites are underlined, and the relevant enzymes are mentioned in parentheses.

After the two plasmids were conjugated into the Δ*csal0990* mutant via biparental mating from *E. coli* S17-1, strains CSΔ0990(pBBR1MCS2-HBL90) and CSΔ0990(pBBR1MCS2-HBS90) were employed for growth experiments to test their phenotype on DMG.

Measurement of ammonium by ion chromatography. The concentration of ammonium was measured using a Dionex ICS-5000+ DC ion chromatography system (Thermo Fisher Scientific, Inc.) equipped with a Dionex IonPac CG12A guard column (4 mm × 50 mm), a Dionex IonPac CS12A analytical column (4 mm × 250 mm), a Dionex CERS 500 cation self-regenerating suppressor (4 mm), an ICS-5000+ conductivity detector, and an AS-AP autosampler. Prior to ion chromatographic analysis, 1 ml of liquid culture was centrifuged to remove the bacterial pellet, and the supernatant was diluted 50-fold with the eluent solution, which contains 22 mM methanesulfonic acid dissolved in water. Subsequently, the diluted sample was filtered across a 0.22-μm nitrocellulose membrane, and then 25 μl of the filtered solution was injected for analysis. Chromatographic separation was carried out at 30°C with the eluent solution at a flow rate of 1.0 ml/min. Data integration and analysis were performed using Dionex Chromeleon 7.2 SR4 software. Calibration curves of ammonium in the concentration range of 0.05 to 0.45 mM were used for quantification.

Expression and purification of His-tagged DdhC (Csal_0990) in *E. coli*. For overproduction of DdhC (GenBank accession number WP_011506293) as an N-terminally 6-histidine-tagged fusion protein (His_6-DdhC), the coding region of *csal_0990* was PCR amplified using the primers N0990F and N0990R and was cloned into the NdeI and HindIII sites of pET28a, yielding pET28-N0990. After the insertion fragment was sequenced to confirm that no mutation was introduced during PCR amplification, the recombinant plasmid was transformed into *E. coli* BL21(DE3) competent cells. Single positive colonies were used to inoculate LB broth containing kanamycin and grown at 37°C with shaking (120 rpm) to an OD_{600} of 0.4 to 0.6. After the cultures were cooled to 25°C, both riboflavin (3.6 μg/ml) and IPTG (0.05 mM) were added to the medium, followed by further incubation at 22 to 25°C with shaking for 12 to 16 h. Cells were harvested by centrifugation, washed twice with ice-cold buffer A (20 mM sodium phosphate buffer [PBS], pH 7.5), and disrupted by sonication on ice for 30 min (200 W, 3-s pulsing and 6-s resting). The entire following purification procedure was performed at 4°C. Cell debris was removed by centrifugation, and the soluble target protein in the supernatant was purified using an Ni-NTA Sefinose resin kit. The

purification procedure was mainly performed according to the manufacturer's instructions, except that the concentrations of imidazole in the washing buffer and elution buffer were optimized to be 30 mM and 200 mM, respectively. The eluted fractions were pooled, concentrated with Amicon Ultra-10 molecular weight cutoff filters (Merck), and dissolved in buffer A. The purified enzyme was stored at 4°C or −40°C in 50% (vol/vol) glycerol.

Polyacrylamide gel electrophoresis and molecular weight determination. The molecular weight of the purified enzyme was determined by sodium dodecyl sulfate-polyacrylamide gel electrophoresis (SDS-PAGE) and gel filtration chromatography. SDS-PAGE was performed according to the protocol described by Laemmli et al. (69). Gel filtration chromatography was performed as described previously (10) with yeast alcohol dehydrogenase (molecular weight, 150,000), bovine serum albumin (66,000), ovalbumin (43,000), and cytochrome *c* from horse heart (12,400) as standard proteins.

For activity staining, purified enzyme was separated at 4°C by native PAGE, which was similar to SDS-PAGE except that SDS and 2-mercaptoethanol were omitted. After electrophoresis, the gel was divided into two parts. One part of the gel was stained with Coomassie brilliant blue R-250, and the other part was soaked in 30 ml of PBS buffer (pH 7.5) containing 20 mM DMG, 2 mM NAD^+, 1 mM PMS, and 2 mM NBT and incubated at room temperature in darkness (to prevent photochemical reduction of NBT) until the band appeared.

Extraction and determination of the prosthetic group. Purified enzyme was boiled for 10 min to release non-covalently bound flavin. After centrifugation, the yellow supernatant and white sediment were collected separately. Aliquots (10 μl) of the supernatant containing the released flavin were analyzed using the Waters e2695 high-performance liquid chromatography (HPLC) system equipped with a 2998 photodiode array (PDA) detector and a Spherisorb S5 ODS2 column (250 mm by 4.6 mm, 5 μm particle size) (Waters Corp., USA). Isocratic elution of samples was carried out with 35% methanol (vol/vol) in 10 mM PBS buffer (pH 6.0) at a flow rate of 1.0 ml/min. Under these conditions, the retention times of authentic FAD and FMN were 7.9 and 11.8 min, respectively. The content of extracted flavin in solution was quantified spectrophotometrically by comparison of the peak area at 450 nm with those of flavin standard solutions (0.1 mM to 1.0 mM FAD), using a molar extinction coefficient of 11.3 mM^{-1} cm^{-1} (70). The white sediment was used to check for the presence of covalently bound flavin with the method described by Sato et al. (71). Absorption spectra of the purified enzyme and the released flavin were recorded using either a UV2301II UV-visible spectrophotometer (Techcomp, Shanghai, China) or a NanoDrop One/One^C spectrophotometer (Gene Co. Ltd.).

Enzyme assays and kinetics. DMGDH activity was measured with the dye-linked assay systems, with PMS as the electron intermediator and DCPIP or NBT as the terminal electron acceptor.

PMS/NBT assay system. The PMS/NBT assay system DMGDH activity was determined in dim light by spectrophotometrically measuring the amount of formazan produced at 570 nm (ε_{570} = 20.1 mM^{-1} · cm^{-1}). The reaction mixtures (1 ml, final volume) contained 20 mM PBS buffer (pH 7.5), 60 mM dimethylglycine, 20 μg PMS, 100 μg NBT, and an appropriate amount of the enzyme. The reactions were started by addition of the purified enzyme. After incubation at 60°C for 10 min, the reaction was quenched by addition of 1 ml of 30 mM HCl, and then the absorbance was measured at 570 nm. One unit of activity was defined as the amount of enzyme catalyzing the formation of 1 μmol of formazan per minute under the assay conditions. Protein concentrations were quantified as described previously (72) with bovine serum albumin as the standard, and specific activity was defined as units per milligram of protein. All the assays were done in triplicate.

PMS/DCPIP assay system. The PMS/DCPIP assay system DMGDH activity was measured spectrophotometrically by monitoring the PMS-mediated reduction of DCPIP (ε_{600} = 20.7 mM^{-1} cm^{-1}) (73). The assay system contained 20 mM PBS (pH 7.5), 60 mM DMG, 4 mM NAD^+, 2.2 mM PMS, 30 μM DCPIP, and enzyme in a final volume of 1 ml. The reaction was started at 25°C by addition of purified enzyme, and then the decrease at 600 nm was followed for 5 min. One unit of enzyme activity is defined as the amount of enzyme required for the reduction of 1 μmol DCPIP per minute under the assay conditions.

The effects of pH on enzyme activity were determined with DMG as a substrate in the following buffers (each at 20 mM): sodium acetate (pH 3.0 to 6.0), sodium phosphate (pH 6.0 to 8.0), Tris-HCl (pH 8.0 to 9.0), and glycine-NaOH (pH 9.0 to 11.0). The optimal temperature was tested at various temperatures ranging from 15 to 60°C at the optimum pH. The thermostability of DdhC was evaluated by incubating the enzyme in 20 mM sodium phosphate buffer (pH 7.5) and measuring the residual activity after various times at temperatures from 40 to 60°C.

For determination of kinetic parameters, different concentrations of DMG (1 to 64 mM), sarcosine (1 to 64 mM), NAD^+ (0.2 to 6.4 mM), and $NADP^+$ (0.2 to 12.8 mM) were tested. Apparent K_m and V_{max} values were obtained by nonlinear fitting Michaelis-Mention equation to the data using Prism 5.0 (GraphPad Software, San Diego, CA).

Analysis of the reaction products. The amounts of DMG and sarcosine in *in vitro* assays were measured at 254 nm using the Waters e2695 HPLC system equipped with a 2998 PDA detector and a Supelcosil LC-SCX column (250 mm by 4.6 mm, 5 μm particle size) (Supelco, Inc.) heated to 30°C, as described previously (10) with some modifications. The mobile phase was 90% (vol/vol) acetonitrile and 10% (vol/vol) choline aqueous solution (22 mM) at a flow rate of 1.0 ml/min. Under the above-described assay conditions, the retention times of authentic DMG and sarcosine were 6.2 and 4.2 min, respectively. Quantitation of DMG and sarcosine in the reaction mixture was accomplished by comparison of the peak areas with those of authentic DMG and sarcosine at known concentrations. The amount of formaldehyde produced in the *in vitro* assay was measured as described by Colby and Zatman (31).

Sequence and phylogenetic analysis. The whole-genome sequence of *C. salexigens* DSM 3043 (GenBank accession number NC_007963.1) was retrieved from the genome databases deposited at the

NCBI website. Homology searches were made using the BLAST program in the European Bioinformatics Institute (EMBL-EBI) website (https://www.ebi.ac.uk/) and the National Center for Biotechnology Information (NCBI) website (https://www.ncbi.nlm.nih.gov/). Conserved domains and sequence motifs in protein sequences were scanned in the NCBI Conserved Domain Search database and the Pfam website (http://pfam.xfam.org/), respectively. Multiple sequence alignment was performed with MultAlin and visualized with ESPript (74). The secondary structure of DdhC was analyzed with the program ThreaDomEx (75). Transmembrane helices and orientation were predicted with the programs TMpred (https://embnet.vital-it.ch/software/TMPRED_form.html) and TMHMM 2.0 (http://www.cbs.dtu.dk/services/TMHMM-2.0/). Phylogenetic trees were constructed using the neighbor-joining method, based on the Jones-Taylor-Thornton model in MEGA X (76) with the bootstrap value set at 1,000 and partial deletion of gaps at 95%.

SUPPLEMENTAL MATERIAL

Supplemental material is available online only.

SUPPLEMENTAL FILE 1, PDF file, 1.6 MB.

ACKNOWLEDGMENTS

This work was financially supported by the National Natural Science Foundation of China (grant number 31070047) and the Major Agricultural Applied Technological Innovation Projects in Shandong Province (grant number SD2019ZZ014).

W.-D.L. designed and supervised the research. T.Y., Y.-H.S., and L.-Z.G. performed the experiments. X.-L.M. and H.Y. analyzed the data. T.Y., Y.-H.S., and W.-D.L. wrote the manuscript.

REFERENCES

1. Smith LT, Pocard JA, Bernard T, Le Rudulier D. 1988. Osmotic control of glycine betaine biosynthesis and degradation in *Rhizobium meliloti*. J Bacteriol 170:3142–3149. https://doi.org/10.1128/jb.170.7.3142-3149.1988.
2. Barra L, Fontenelle C, Ermel G, Trautwetter A, Walker GC, Blanco C. 2006. Interrelations between glycine betaine catabolism and methionine biosynthesis in *Sinorhizobium meliloti* strain 102F34. J Bacteriol 188:7195–7204. https://doi.org/10.1128/JB.00208-06.
3. Wargo MJ. 2013. Homeostasis and catabolism of choline and glycine betaine: lessons from *Pseudomonas aeruginosa*. Appl Environ Microbiol 79:2112–2120. https://doi.org/10.1128/AEM.03565-12.
4. Figueroa-Soto CG, Valenzuela-Soto EM. 2018. Glycine betaine rather than acting only as an osmolyte also plays a role as regulator in cellular metabolism. Biochimie 147:89–97. https://doi.org/10.1016/j.biochi.2018.01.002.
5. Möller B, Hippe H, Gottschalk G. 1986. Degradation of various amine compounds by mesophilic clostridia. Arch Microbiol 145:85–90. https://doi.org/10.1007/BF00413032.
6. Meyer M, Granderath K, Andreesen JR. 1995. Purification and characterization of protein PB of betaine reductase and its relationship to the corresponding proteins glycine reductase and sarcosine reductase from *Eubacterium acidaminophilum*. Eur J Biochem 234:184–191. https://doi.org/10.1111/j.1432-1033.1995.184_c.x.
7. Müller E, Fahlbusch K, Walther R, Gottschalk G. 1981. Formation of *N,N*-dimethylglycine, acetic acid, and butyric acid from betaine by *Eubacterium limosum*. Appl Environ Microbiol 42:439–445. https://doi.org/10.1128/AEM.42.3.439-445.1981.
8. Watkins AJ, Roussel EG, Parkes RJ, Sass H. 2014. Glycine betaine as a direct substrate for methanogens (Methanococcoides spp.). Appl Environ Microbiol 80:289–293. https://doi.org/10.1128/AEM.03076-13.
9. Lechtenfeld M, Heine J, Sameith J, Kremp F, Müller V. 2018. Glycine betaine metabolism in the acetogenic bacterium *Acetobacterium woodii*. Environ Microbiol 20:4512–4525. https://doi.org/10.1111/1462-2920.14389.
10. Shao Y-H, Guo L-Z, Zhang Y-Q, Yu H, Zhao B-S, Pang H-Q, Lu W-D. 2018. Glycine betaine monooxygenase, an unusual Rieske-type oxygenase system, catalyzes the oxidative *N*-demethylation of glycine betaine in *Chromohalobacter salexigens* DSM 3043. Appl Environ Microbiol 84:e00377-18. https://doi.org/10.1128/AEM.00377-18.
11. Mori N, Kawakami B, Tani Y, Yamada H. 1980. Purification and properties of dimethylglycine oxidase from *Cylindrocarpon didymum* M–1. Agric Biol Chem 44:1383–1389. https://doi.org/10.1271/bbb1961.44.1383.
12. Meskys R, Harris RJ, Casaite V, Basran J, Scrutton NS. 2001. Organization of the genes involved in dimethylglycine and sarcosine degradation in *Arthrobacter* spp.: implications for glycine betaine catabolism. Eur J Biochem 268:3390–3398. https://doi.org/10.1046/j.1432-1327.2001.02239.x.
13. Oka I, Yoshimoto T, Rikitake K, Ogushi S, Tsuru D. 1979. Sarcosine dehydrogenase from *Pseudomonas putida*: purification and some properties. Agric Biol Chem 43:1197–1203. https://doi.org/10.1271/bbb1961.43.1197.
14. Hinton RJ, Atkinson T, Price CP, Scawen MD. 1990. Purification and characterization of sarcosine dehydrogenase, p 355–363. *In* Pyle DL (ed), Separations for biotechnology 2. Springer Netherlands, Dordrecht, The Netherlands. https://doi.org/10.1007/978-94-009-0783-6_38.
15. Trickey P, Wagner MA, Jorns MS, Mathews FS. 1999. Monomeric sarcosine oxidase: structure of a covalently flavinylated amine oxidizing enzyme. Structure 7:331–345. https://doi.org/10.1016/S0969-2126(99)80043-4.
16. Chen ZW, Hassan-Abdulah A, Zhao G, Jorns MS, Mathews FS. 2006. Heterotetrameric sarcosine oxidase: structure of a diflavin metalloenzyme at 1.85 Å resolution. J Mol Biol 360:1000–1018. https://doi.org/10.1016/j.jmb.2006.05.067.
17. Binzak BA, Wevers RA, Moolenaar SH, Lee Y-M, Hwu W-L, Poggi-Bach J, Engelke UFH, Hoard HM, Vockley JG, Vockley J. 2001. Cloning of dimethylglycine dehydrogenase and a new human inborn error of metabolism, dimethylglycine dehydrogenase deficiency. Am J Hum Genet 68:839–847. https://doi.org/10.1086/319520.
18. García-Estepa R, Cánovas D, Iglesias-Guerra F, Ventosa A, Csonka LN, Nieto JJ, Vargas C. 2006. Osmoprotection of *Salmonella enterica* serovar Typhimurium by *N*γ-acetyldiaminobutyrate, the precursor of the compatible solute ectoine. Syst Appl Microbiol 29:626–633. https://doi.org/10.1016/j.syapm.2006.01.008.
19. Meadows JA, Wargo MJ. 2015. Carnitine in bacterial physiology and metabolism. Microbiology 161:1161–1174. https://doi.org/10.1099/mic.0.000080.
20. Park S, Smith LT, Smith GM. 1995. Role of glycine betaine and related osmolytes in osmotic stress adaptation in *Yersinia enterocolitica* ATCC 9610. Appl Environ Microbiol 61:4378–4381. https://doi.org/10.1128/AEM.61.12.4378-4381.1995.
21. Bashir A, Hoffmann T, Smits SHJ, Bremer E. 2014. Dimethylglycine provides salt and temperature stress protection to *Bacillus subtilis*. Appl Environ Microbiol 80:2773–2785. https://doi.org/10.1128/AEM.00078-14.
22. Arahal DR, Garcia MT, Vargas C, Canovas D, Nieto JJ, Ventosa A. 2001. *Chromohalobacter salexigens* sp. nov., a moderately halophilic species that includes *Halomonas elongata* DSM 3043 and ATCC 33174. Int J Syst

Evol Microbiol 51:1457–1462. https://doi.org/10.1099/00207713-51-4-1457.
23. García-Estepa R, Argandona M, Reina-Bueno M, Capote N, Iglesias-Guerra F, Nieto JJ, Vargas C. 2006. The *ectD* gene, which is involved in the synthesis of the compatible solute hydroxyectoine, is essential for thermoprotection of the halophilic bacterium *Chromohalobacter salexigens*. J Bacteriol 188:3774–3784. https://doi.org/10.1128/JB.00136-06.
24. Shao YH, Guo LZ, Yu H, Zhao BS, Lu WD. 2017. Establishment of a markerless gene deletion system in *Chromohalobacter salexigens* DSM 3043. Extremophiles 21:839–850. https://doi.org/10.1007/s00792-017-0946-y.
25. Calderón MI, Vargas C, Rojo F, Iglesias-Guerra F, Csonka LN, Ventosa A, Nieto JJ. 2004. Complex regulation of the synthesis of the compatible solute ectoine in the halophilic bacterium *Chromohalobacter salexigens* DSM 3043^T. Microbiology 150:3051–3063. https://doi.org/10.1099/mic.0.27122-0.
26. Wargo MJ, Szwergold BS, Hogan DA. 2008. Identification of two gene clusters and a transcriptional regulator required for *Pseudomonas aeruginosa* glycine betaine catabolism. J Bacteriol 190:2690–2699. https://doi.org/10.1128/JB.01393-07.
27. Kleiger G, Eisenberg D. 2002. GXXXG and GXXXA motifs stabilize FAD and NAD(P)-binding Rossmann folds through Cα–H···O hydrogen bonds and van der Waals interactions. J Mol Biol 323:69–76. https://doi.org/10.1016/S0022-2836(02)00885-9.
28. George DG, Hunt LT, Yeh LSL, Barker WC. 1985. New perspectives on bacterial ferredoxin evolution. J Mol Evol 22:20–31. https://doi.org/10.1007/BF02105801.
29. Wang R, Yi J, Shang J, Yu W, Li Z, Huang H, Xie H, Wang S. 2019. 6-hydroxypseudooxynicotine dehydrogenase delivers electrons to electron transfer flavoprotein during nicotine degradation by *Agrobacterium tumefaciens* S33. Appl Environ Microbiol 85:e00454-19. https://doi.org/10.1128/AEM.00454-19.
30. Vargas C, Jebbar M, Carrasco R, Blanco C, Calderon MI, Iglesias-Guerra F, Nieto JJ. 2006. Ectoines as compatible solutes and carbon and energy sources for the halophilic bacterium *Chromohalobacter salexigens*. J Appl Microbiol 100:98–107. https://doi.org/10.1111/j.1365-2672.2005.02757.x.
31. Colby J, Zatman LJ. 1974. Purification and properties of the trimethylamine dehydrogenase of bacterium 4B6. Biochem J 143:555–567. https://doi.org/10.1042/bj1430555.
32. Singer TP, Edmondson DE. 1978. Flavoproteins (overview), p 397–418. *In* Fleischer S, Packer L (ed), Methods in enzymology, vol 53. Academic Press, San Diego, CA.
33. Moulis JM, Sieker LC, Wilson KS, Dauter Z. 1996. Crystal structure of the 2[4Fe-4S] ferredoxin from *Chromatium vinosum*: evolutionary and mechanistic inferences for [3/4Fe-4S] ferredoxins. Protein Sci 5:1765–1775. https://doi.org/10.1002/pro.5560050902.
34. Yoon KS, Bobst C, Hemann C, Hille R, Tabita FR. 2001. Spectroscopic and functional properties of novel 2[4Fe-4S] cluster-containing ferredoxins from the green sulfur bacterium *Chlorobium tepidum*. J Biol Chem 276:44027–44036. https://doi.org/10.1074/jbc.M107852200.
35. Aliverti A, Zanetti G. 1997. A three-domain iron-sulfur flavoprotein obtained through gene fusion of ferredoxin and ferredoxin-NADP$^+$ reductase from spinach leaves. Biochemistry 36:14771–14777. https://doi.org/10.1021/bi971791t.
36. Hoskins DD, Mackenzie CG. 1961. Solubilization and electron transfer flavoprotein requirement of mitochondrial sarcosine dehydrogenase and dimethylglycine dehydrogenase. J Biol Chem 236:177–183.
37. Hoskins DD, Bjur RA. 1965. The electron-transferring flavoprotein of primate liver mitochondria. Purification of the enzyme and reconstitution of the sarcosine oxidase system. J Biol Chem 240:2201–2208.
38. Watmough NJ, Frerman FE. 2010. The electron transfer flavoprotein: ubiquinone oxidoreductases. Biochim Biophys Acta 1797:1910–1916. https://doi.org/10.1016/j.bbabio.2010.10.007.
39. Hubbard PA, Liang X, Schulz H, Kim J. 2003. The crystal structure and reaction mechanism of *Escherichia coli* 2,4-dienoyl-CoA reductase. J Biol Chem 278:37553–37560. https://doi.org/10.1074/jbc.M304642200.
40. Scrutton NS, Sutcliffe MJ. 2000. Trimethylamine dehydrogenase and electron transferring flavoprotein. Subcell Biochem 35:145–181. https://doi.org/10.1007/0-306-46828-x_5.
41. Mittl PR, Schulz GE. 1994. Structure of glutathione reductase from *Escherichia coli* at 1.86 Å resolution: comparison with the enzyme from human erythrocytes. Protein Sci 3:799–809. https://doi.org/10.1002/pro.5560030509.
42. Barber M, Neame PJ, Lim LW, White S, Matthews FS. 1992. Correlation of X-ray deduced and experimental amino acid sequences of trimethylamine dehydrogenase. J Biol Chem 267:6611–6619.
43. Yang CC, Packman LC, Scrutton NS. 1995. The primary structure of *Hyphomicrobium* X dimethylamine dehydrogenase. Eur J Biochem 232:264–271. https://doi.org/10.1111/j.1432-1033.1995.tb20808.x.
44. Limburg J, Mure M, Klinman JP. 2005. Cloning and characterization of histamine dehydrogenase from *Nocardioides simplex*. Arch Biochem Biophys 436:8–22. https://doi.org/10.1016/j.abb.2004.11.024.
45. Reed T, Lushington GH, Xia Y, Hirakawa H, Travis DM, Mure M, Scott EE, Limburg J. 2010. Crystal structure of histamine dehydrogenase from *Nocardioides simplex*. J Biol Chem 285:25782–25791. https://doi.org/10.1074/jbc.M109.084301.
46. Lim LW, Shamala N, Mathews FS, Steenkamp DJ, Hamlin R, Xuong NH. 1986. Three-dimensional structure of the iron-sulfur flavoprotein trimethylamine dehydrogenase at 2.4-Å resolution. J Biol Chem 261:15140–15146.
47. Netz DJA, Pierik AJ, Stümpfig M, Bill E, Sharma AK, Pallesen LJ, Walden WE, Lill R. 2012. A bridging [4Fe-4S] cluster and nucleotide binding are essential for function of the Cfd1-Nbp35 complex as a scaffold in iron-sulfur protein maturation. J Biol Chem 287:12365–12378. https://doi.org/10.1074/jbc.M111.328914.
48. Phillips DA, Sande ES, Vriezen JAC, de Bruijn FJ, Le Rudulier D, Joseph CM. 1998. A new genetic locus in *Sinorhizobium meliloti* is involved in stachydrine utilization. Appl Environ Microbiol 64:3954–3960. https://doi.org/10.1128/AEM.64.10.3954-3960.1998.
49. Liu XL, Scopes RK. 1993. Cloning, sequencing and expression of the gene encoding NADH oxidase from the extreme anaerobic thermophile *Thermoanaerobium brockii*. Biochim Biophys Acta 1174:187–190. https://doi.org/10.1016/0167-4781(93)90113-R.
50. Li Z, Kim DD, Nelson OD, Otwell AE, Richardson RE, Callister SJ, Lin H. 2015. Molecular dissection of a putative iron reductase from *Desulfotomaculum reducens* MI-1. Biochem Biophys Res Commun 467:503–508. https://doi.org/10.1016/j.bbrc.2015.10.016.
51. Kang DJ, Ridlon JM, Moore DR, Barnes S, Hylemon PB. 2008. *Clostridium scindens baiCD* and *baiH* genes encode stereo-specific 7α/7β-hydroxy-3-oxo-Δ4-cholenoic acid oxidoreductases. Biochim Biophys Acta 1781:16–25. https://doi.org/10.1016/j.bbalip.2007.10.008.
52. Dickert S, Pierik AJ, Linder D, Buckel W. 2000. The involvement of coenzyme A esters in the dehydration of (R)-phenyllactate to (E)-cinnamate by *Clostridium sporogenes*. Eur J Biochem 267:3874–3884. https://doi.org/10.1046/j.1432-1327.2000.01427.x.
53. Fitzpatrick PF. 2013. (6) Amine and amino acid oxidases and dehydrogenases, p 119–138. *In* Hille R, Miller S, Palfey B (ed), Handbook of flavoproteins, vol 1. Oxidases, dehydrogenases and related systems. Walter de Gruyter GmbH, Berlin, Germany.
54. Lang H, Polster M, Brandsch R. 1991. Rat liver dimethylglycine dehydrogenase. Eur J Biochem 198:793–799. https://doi.org/10.1111/j.1432-1033.1991.tb16083.x.
55. Cook RJ, Wagner C. 1986. Dimethylglycine dehydrogenase and sarcosine dehydrogenase: mitochondrial folate-binding proteins from rat liver. Methods Enzymol 122:255–260. https://doi.org/10.1016/0076-6879(86)22179-5.
56. Luka Z, Pakhomova S, Loukachevitch LV, Newcomer ME, Wagner C. 2014. Folate in demethylation: the crystal structure of the rat dimethylglycine dehydrogenase complexed with tetrahydrofolate. Biochem Biophys Res Commun 449:392–398. https://doi.org/10.1016/j.bbrc.2014.05.064.
57. Leys D, Basran J, Scrutton NS. 2003. Channelling and formation of 'active' formaldehyde in dimethylglycine oxidase. EMBO J 22:4038–4048. https://doi.org/10.1093/emboj/cdg395.
58. Porter DH, Cook RJ, Wagner C. 1985. Enzymatic properties of dimethylglycine dehydrogenase and sarcosine dehydrogenase from rat liver. Arch Biochem Biophys 243:396–407. https://doi.org/10.1016/0003-9861(85)90516-8.
59. Csonka LN, Hanson AD. 1991. Prokaryotic osmoregulation: genetics and physiology. Annu Rev Microbiol 45:569–606. https://doi.org/10.1146/annurev.mi.45.100191.003033.
60. Lu WD, Chi ZM, Su CD. 2006. Identification of glycine betaine as compatible solute in *Synechococcus* sp. WH8102 and characterization of its *N*-methyltransferase genes involved in betaine synthesis. Arch Microbiol 186:495–506. https://doi.org/10.1007/s00203-006-0167-8.
61. Nyyssölä A, Kerovuo J, Kaukinen P, von Weymarn N, Reinikainen T. 2000. Extreme halophiles synthesize betaine from glycine by meth-

ylation. J Biol Chem 275:22196–22201. https://doi.org/10.1074/jbc.M910111199.
62. Lai MC, Yang DR, Chuang MJ. 1999. Regulatory factors associated with synthesis of the osmolyte glycine betaine in the halophilic methanoarchaeon *Methanohalophilus portucalensis*. Appl Environ Microbiol 65:828–833. https://doi.org/10.1128/AEM.65.2.828-833.1999.
63. Cánovas D, Vargas C, Iglesias-Guerra F, Csonka LN, Rhodes D, Ventosa A, Nieto JJ. 1997. Isolation and characterization of salt-sensitive mutants of the moderate halophile *Halomonas elongata* and cloning of the ectoine synthesis genes. J Biol Chem 272:25794–25801. https://doi.org/10.1074/jbc.272.41.25794.
64. Nyyssölä A, Reinikainen T, Leisola M. 2001. Characterization of glycine sarcosine *N*-methyltransferase and sarcosine dimethylglycine *N*-methyltransferase. Appl Environ Microbiol 67:2044–2050. https://doi.org/10.1128/AEM.67.5.2044-2050.2001.
65. Sambrook J, Fritsch EF, Maniatis T. 1989. Molecular cloning: a laboratory manual, 2nd ed. Cold Spring Harbor Laboratory Press, Cold Spring Harbor, NY.
66. Cánovas D, Borges N, Vargas C, Ventosa A, Nieto JJ, Santos H. 1999. Role of Nγ-acetyldiaminobutyrate as an enzyme stabilizer and an intermediate in the biosynthesis of hydroxyectoine. Appl Environ Microbiol 65:3774–3779. https://doi.org/10.1128/AEM.65.9.3774-3779.1999.
67. Heckman KL, Pease LR. 2007. Gene splicing and mutagenesis by PCR-driven overlap extension. Nat Protoc 2:924–932. https://doi.org/10.1038/nprot.2007.132.
68. Kovach ME, Elzer PH, Steven Hill D, Robertson GT, Farris MA, Roop MR II, Peterson KM. 1995. Four new derivatives of the broad-host-range cloning vector pBBR1MCS, carrying different antibiotic-resistance cassettes. Gene 166:175–176. https://doi.org/10.1016/0378-1119(95)00584-1.
69. Laemmli UK. 1970. Cleavage of structural proteins during the assembly of the head of bacteriophage T4. Nature 227:680–685. https://doi.org/10.1038/227680a0.
70. Whitby LG. 1953. A new method for preparing flavin-adenine dinucleotide. Biochem J 54:437–442. https://doi.org/10.1042/bj0540437.
71. Sato M, Ohishi N, Nishikimi M, Yagi K. 1977. Proteins with covalently-bound flavin in rat liver mitochondria. Biochem Biophys Res Commun 78:868–873. https://doi.org/10.1016/0006-291X(77)90503-4.
72. Bradford MM. 1976. A rapid and sensitive method for the quantitation of microgram quantities of protein utilizing the principle of protein-dye binding. Anal Biochem 72:248–254. https://doi.org/10.1016/0003-2697(76)90527-3.
73. Armstrong JM. 1964. The molar extinction coefficient of 2,6-dichlorophenol indophenol. Biochim Biophys Acta 86:194–197. https://doi.org/10.1016/0304-4165(64)90180-1.
74. Robert X, Gouet P. 2014. Deciphering key features in protein structures with the new ENDscript server. Nucleic Acids Res 42:W320–W324. https://doi.org/10.1093/nar/gku316.
75. Wang Y, Wang J, Li R, Shi Q, Xue Z, Zhang Y. 2017. ThreaDomEx: a unified platform for predicting continuous and discontinuous protein domains by multiple-threading and segment assembly. Nucleic Acids Res 45:W400–W407. https://doi.org/10.1093/nar/gkx410.
76. Kumar S, Stecher G, Tamura K. 2016. MEGA7: Molecular Evolutionary Genetics Analysis version 7.0 for bigger datasets. Mol Biol Evol 33:1870–1874. https://doi.org/10.1093/molbev/msw054.